Journal of Nanobiotechnology

RESEARCH

Open Access

Development of NIR photocleavable nanoparticles with BDNF for vestibular neuron regeneration

Celine DG. Abueva[1,2†], Sung Ryeong Yoon[3†], Nathaniel T. Carpena[3], Seung Cheol Ahn[4], So-Young Chang[1,2], Ji Eun Choi[5], Min Young Lee[5*] and Jae Yun Jung[5*]

Abstract

Among nanoparticle platforms, light or photoresponsive nanoparticles have emerged as a promising drug delivery strategy with spatiotemporal control while minimizing off-target effects. The characteristic absorption spectrum of the photoresponsive moiety dictates the wavelength of light needed to activate bond cleavage. However, the low tissue penetration depth limit and short-wavelength ultraviolet (UV) cellular toxicity are considered disadvantageous. This study developed a vestibular ganglion neuron organoid as a model for vestibulopathy. UV and near-infrared (NIR) radiation targeted the inner ear and neural cells, followed by toxicity evaluation. A significantly smaller toxicity of NIR light was confirmed. The photocleavage release of brain-derived neurotrophic factor (BDNF) was used by applying NIR wavelength. The results indicate that polyethylene glycol octamethylene diamine derivative conjugated with leucomethylene blue with an ethanolamine linker nanoparticle can be effectively disassembled and release BDNF when using the 808 nm laser as a trigger. The findings of the cytotoxicity assay suggest that photocleavable nanoparticles (PCNs) and laser irradiation are safe and biocompatible for human-derived and neural progenitor types of cells. Phototriggered BDNF release by NIR laser supported the growth and differentiation of human neural progenitor cells in culture. In addition, the vestibulopathy organoid exhibited a significant regenerative effect. This study harnesses the full potential of NIR laser PCNs to treat vestibular neuropathies.

†Celine DG. Abueva and Sung Ryeong Yoon contributed equally to this work.

*Correspondence:
Min Young Lee
eyeglass210@gmail.com
Jae Yun Jung
jjkingy2k@gmail.com

Full list of author information is available at the end of the article

Graphical abstract

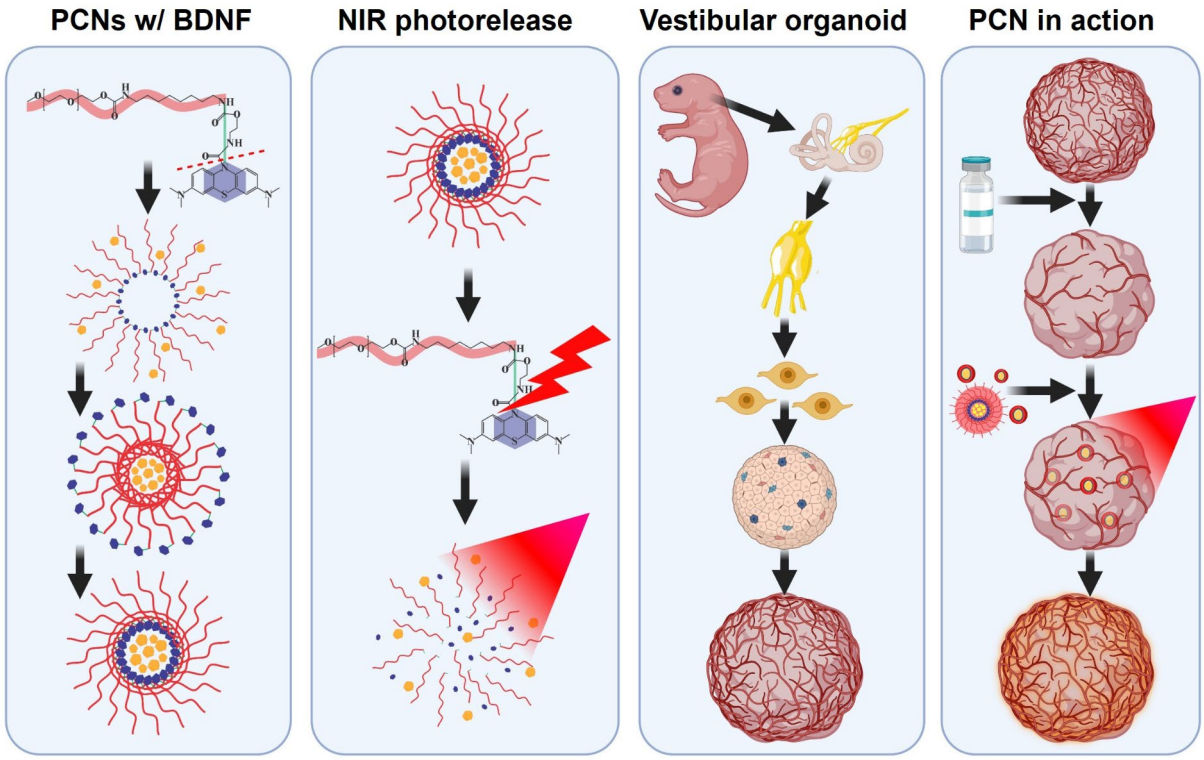

Keywords Photocleavage, Nanoparticle, Near-infrared, BDNF, Vestibular organoid

Introduction

Nanoparticles represent a cutting-edge frontier in drug delivery technology, offering a myriad of advantages for targeted therapeutic interventions. These nanoscale carriers, typically ranging from 1 to 100 nm in size, exhibit unique properties that make them ideal candidates for addressing complex medical conditions [1]. In inner ear neuropathies, nanoparticle-based drug delivery systems hold particular promise, offering a novel approach to overcoming the challenges associated with conventional treatment methods.

One of the most intriguing aspects of nanoparticles is their versatility in design and function. Nanoparticles can be engineered with precision at the molecular level, tailored to meet specific therapeutic needs, including controlled drug release, targeted delivery, and enhanced bioavailability [2]. Surface modifications allow for precise tuning of physicochemical properties, such as charge, hydrophobicity, and biocompatibility, ensuring optimal interactions with biological systems.

Among nanoparticle platforms, light or photoresponsive nanoparticles have emerged as a promising drug delivery strategy [3]. These nanoparticles are designed to respond to external stimuli, such as light of a specific wavelength, triggering the release of encapsulated therapeutic agents in a controlled manner. The ability to remotely activate drug release offers unprecedented spatiotemporal control, allowing for precise targeting of affected tissues while minimizing systemic exposure and off-target effects.

The inner ear is divided into two different systems, i.e., the cochleae (hearing organ) and the vestibule (balance organ). Both organs are composed of sensory parts that transfer mechanical stimuli to electric and neural parts, which in turn transmit electric signals to the brain. The crucial component of these two organs' sensory parts is hair cells with limited regeneration capacity [4]. Most cochlear pathologies are considered to be related to hair cell pathologies [5]. Hence, rehabilitation devices, such as cochlear implants, have been developed to bypass the hair cells and stimulate the auditory neurons directly. In the case of vestibulopathies, a widely used diagnosis for patients with dizziness and imbalance, dysfunctions occur in various anatomical locations in the vestibular system. The vestibular neuron is one of the most prominent anatomical locations [6–8]. Therefore, developing therapeutic agents to regenerate damaged vestibular neurons could greatly aid patients with vestibulopathy.

Animal models and functional assessment methods for hearing loss are well established, and it is possible to distinguish neural from sensory pathologies [9]. However, behavioral or functional tests for evaluating balance problems are less specific and hardly distinguish neural from sensory vestibulopathy. In addition, acquiring the histologic sample is rather challenging due to the anatomical location of the target organ. Therefore, researchers must develop a specific vestibular damage model to evaluate new or potential therapeutic agents, such as nanoparticles, for regenerating vestibular neurons. Organoids offer several advantages over animal models [10]. One of the most crucial advantages of using organoids as a disease model is enabling the study of a single organ without any influence on surrounding organs or tissue. In this study, a vestibular ganglion neuron organoid was developed for a vestibulopathy disease model. To use this organoid as a specific vestibulopathy disease model, achieving therapeutic effects with spatiotemporal control required a meticulously designed photoresponsive nanoparticle.

The design of therapeutic, photoresponsive nanoparticles involves carefully considering several key factors, including the choice of nanoparticle material, the method of drug encapsulation, and the mechanism of photoresponsiveness [4]. Common materials used for nanoparticles include polymers, lipids, and inorganic compounds. For example, polyethylene glycol (PEG) has been used in biocompatible and efficient delivery systems [11]. Nanoparticles must be biocompatible, stable, and capable of efficiently encapsulating therapeutic payloads, such as brain-derived neurotrophic factor (BDNF), essential in differentiating vestibular neurons [12–14]. The encapsulation of therapeutic agents within nanoparticles can be achieved through various techniques, including physical encapsulation, chemical conjugation, and electrostatic interactions [5]. These methods ensure the efficient loading of drugs into nanoparticles while maintaining their stability and preventing premature release. With BDNF delivery, ensuring the stability and bioactivity of the protein within the nanoparticle matrix is crucial for therapeutic efficacy. The use of photoresponsive nanoparticles carrying BDNF could be vital to treating vestibulopathy.

The phototriggered release mechanism of a load, such as BDNF, from nanoparticles can vary depending on the desired release profile and application. Common strategies include exploiting photochemical reactions, photothermal effects, or photophysical processes triggered by specific wavelengths of light [15]. The choice of phototriggered release mechanism depends on factors such as the desired release kinetics, tissue penetration depth, and compatibility with biological systems. In this study, photocleavage release of BDNF was used to treat vestibulopathy. During photocleavage, photoremovable groups absorb photons and convert energy to trigger bond cleavage. Small photoresponsive moieties can be covalently linked to molecules or nanoparticles and removed by light irradiation to expose targeting ligands or release payloads [16]. Most of all, the characteristic absorption spectrum of the photoresponsive moiety dictates the wavelength of light needed to activate bond cleavage, such as ultraviolet (UV). However, low tissue penetration depth and potential tissue toxicity limit short-wavelength UV light application. Near-infrared (NIR) has been applied in several studies, but only in combination with specific nanoparticle that can transfer the NIR to UV [17, 18]. Eventually, this transferred UV could affect the survival of remaining or regenerated tissue. Thus, there is interest in developing ideal photocleavage strategies using exclusive NIR light to realize photoresponsive payload delivery to deep tissues and promote its clinical applications.

In inner ear neuropathies, photocleavable nanoparticles (PCNs) offer several distinct advantages. These nanoparticles can deliver therapeutic agents directly to the affected tissues within the cochlea and vestibular system by leveraging precise control of phototriggered release. This targeted approach minimizes systemic exposure and reduces the risk of adverse effects while maximizing therapeutic efficacy and patient compliance [19]. One of the most significant obstacles to the delivery of therapeutics into the inner ear is penetration. Since the inner ear is located deep inside, light energy is more suitable for the controlled release of therapeutic agents. The optimal wavelength for inner ear delivery is > 800 nm for the deepest penetration [20]. However, previous reports employing PCNs for the inner ear used UV light, and we could identify no study using wavelengths in the range of > 800 nm. Therefore, developing PCNs for inner ear neuropathies that use deeply penetrating wavelengths that are readily formulated with no biological complications is crucial.

Through interdisciplinary collaboration between materials science, nanotechnology, and otolaryngology researchers, this study aims to harness the full potential of PCNs to treat vestibular neuropathies. By elucidating the mechanisms underlying nanoparticle-mediated drug delivery and optimizing nanoparticle design for clinical applications, this research endeavors to translate scientific advancements into tangible clinical solutions, ultimately improving the quality of life of individuals affected by inner ear disorders, specifically vestibular neurons.

Results

Comparison of cytotoxicity of NIR laser (808 nm) and UV (254 nm) in human neural progenitor cells (hNPCs)

Human neural progenitor cells (hNPCs) were used as a model for resident neural precursor cells in the vestibular

ganglion, which could regenerate the vestibular neuron. In epifluorescence analysis, hNPCs vividly expressed SOX1 and Nestin, which are neural progenitor markers (Fig. 1a). hNPCs proliferated in a culture medium for 3 days, and light irradiations of NIR laser (808 nm) and UV (254 nm) were applied 24 h later. Both light irradiations were performed in three different energy densities (30, 60, and 90 J/cm^2). UV irradiation results show a statistically significant reduction of cell viability at all energy densities (Fig. 1b). NIR laser irradiations show no reduction of cell viability at all densities (Fig. 1c). These results implicate the possibility that UV irradiation, which is most widely adopted (directly or indirectly) as a stimulus for photocleavage, is potentially harmful to resident neural precursor cells in inner ear ganglions.

Development and analysis of the photocleavable polymer

An NIR-photocleavable polymer was developed in this study as a delivery vehicle for BDNF due to the advantageous characteristics of NIR compared with UV and visible light in terms of deeper tissue penetration and reduced phototoxicity. The design utilizes methylene blue (MB), chemically modified at the carbamoyl site, as a photocleavable ligand in the far-red-to-NIR region. MB was reduced to leucomethylene blue (LMB) and conjugated to hydrophilic polyethylene glycol (PEG) to modulate the optical properties and hydrophobicity, forming an amphiphilic polymer. Specifically, LMB was conjugated to a polyethylene glycol octamethylene diamine (PEGOD) derivative via an ethanolamine (EA) linker, resulting in the amphiphilic polymer PEGOD-EA-LMB photocleavable property (Fig. 2a). The synthesized amphiphilic polymer PEGOD-EA-LMB was characterized by proton nuclear magnetic resonance (^{1}H NMR) and Fourier transform-infrared (FT-IR) analyses to confirm its chemical structure and composition. The ^{1}H NMR analysis revealed the presence of peaks corresponding to the different chemical groups in PEGOD-EA-LMB (Fig. 2b), confirming its successful synthesis. Characteristic signals were observed at 6.8 ppm for the LMB ring and at 2.7 ppm for the 12 H of the LMB methyl groups. EA linker CH_2 peaks at 3.4 and 4.3 ppm and 11 C of PEGOD chain peaks at 1.4 ppm were also evident. Based on the ratio of protons on the end groups to

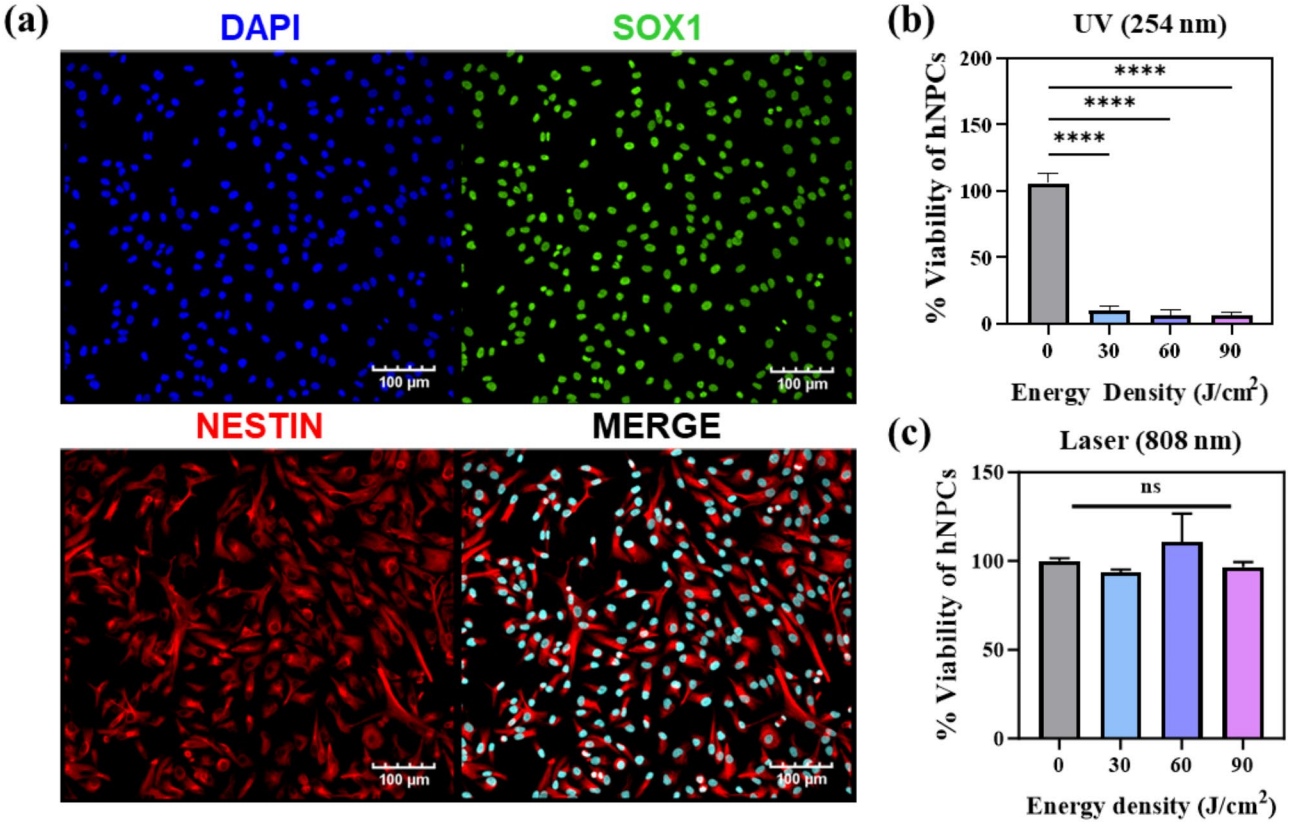

Fig. 1 UV (254 nm) vs. laser (808 nm) cytotoxicity assay in human neural progenitor cells (hNPCs). (**a**) hNPCs were grown in culture for 3 days prior to UV or laser treatment, and viability assays were performed 24 h after. Immunofluorescence images show the expression of NPC markers SOX1 and Nestin. (**b**) UV irradiation at energy densities 30, 60, & 90 J/cm^2 significantly decreased the viability of hNPCs after 24 h in a culture determined via CCK-8 assay. (**c**) Laser irradiation at energy densities 30, 60, & 90 J/cm^2 did not affect hNPCs viability. The statistical significance of the data was analyzed using one-way ANOVA with Tukey's multiple comparisons test for each group (**** $P < 0.0001$)

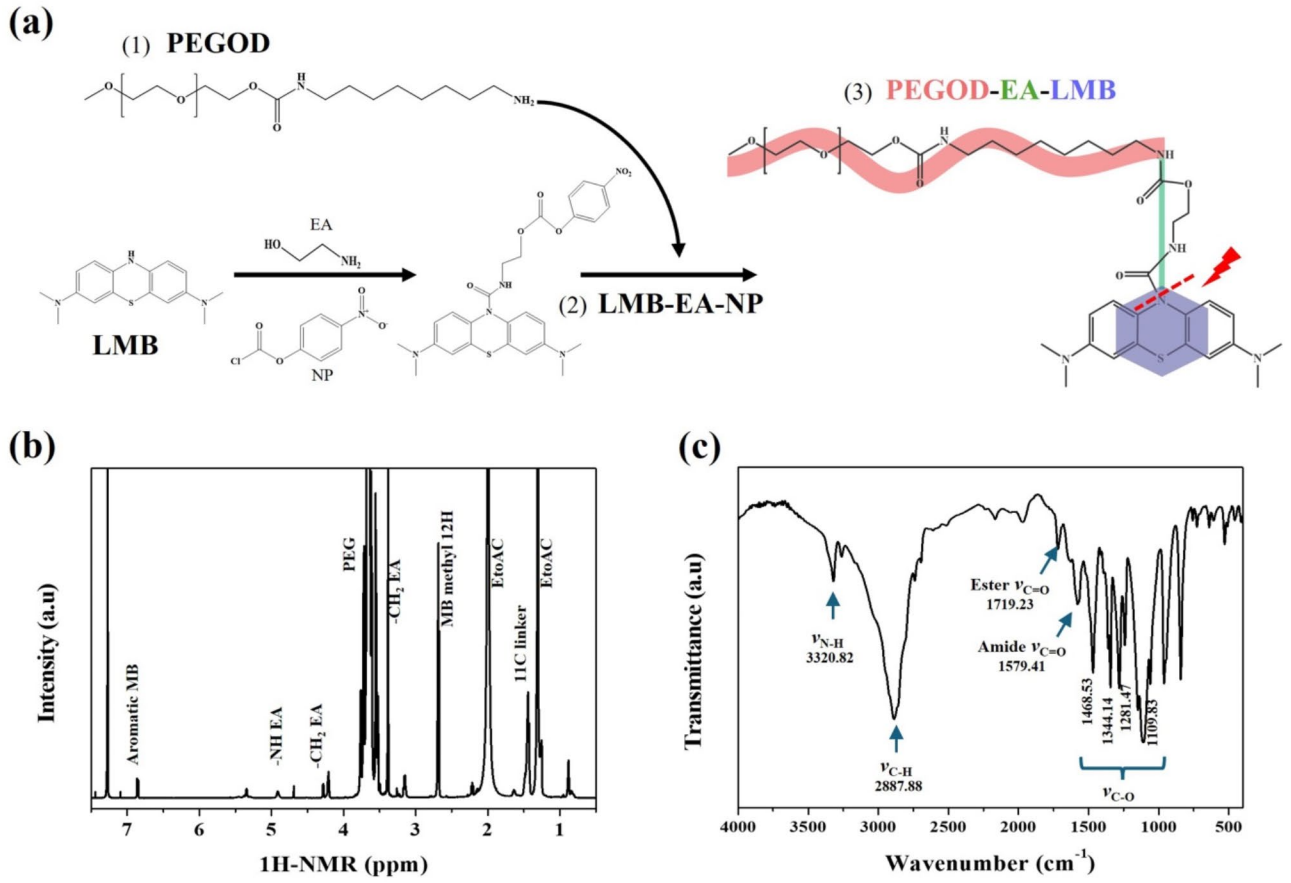

Fig. 2 Photocleavable PEGOD-EA-LMB synthesis. (**a**) Synthesis scheme of polyethylene glycol octamethylene diamine (PEGOD, red) derivative and leucomethylene blue (LMB, blue), linked with ethanolamine (EA, green). The resulting product (PEGOD-EA-LMB) was analyzed, and the structure was confirmed by (**b**) proton nuclear magnetic resonance (600 MHz; $CDCl_3$; δ ppm: 7.24) and (c) Fourier transform-infrared (400–4,000 cm^{-1}) spectroscopy

protons on the polymer chain from the ^1H NMR spectra, the average molecular weight of the synthesized polymer was estimated at 5,795.84 ± 201.63 g/mol (5.8 kDa; S1). Additionally, FT-IR analysis provided evidence of the chemical structure and composition of PEGOD-EA-LMB (Fig. 2c). Its FT-IR spectrum showed the presence of bands corresponding to amide (1,579.41 cm^{-1}) and ester (1,719.23 cm^{-1}) C = O stretching, C–O (1,100–1,470 cm^{-1}) stretching, asymmetrical stretching of C–H in the methyl group (2,887.88 cm^{-1}), and amine stretching (3,320.82 cm^{-1}).

Characteristics of the photocleavable nanoparticles

PEGOD-EA-LMB demonstrated its amphiphilic nature by self-assembling into nanoparticles (Fig. 3a) in aqueous solutions containing BDNF. BDNF was successfully trapped through polymer intercalation when PEGOD-EA-LMB transitioned from aqueous to organic to aqueous solutions and evaporation, creating stable photocleavable nanoparticles. The formed nanoparticle consisted of a hydrophobic LMB core and hydrophilic PEGOD tail with a diameter ranging from 50 to 100 nm, as observed in transmission electron microscopy (TEM) images (Fig. 3b). The self-assembly of PEGOD-EA-LMB with encapsulated BDNF into nanoparticles in aqueous solutions provides a promising delivery system for growth factors in the inner ear. The encapsulation efficiency (EE) of the amphiphilic nanoparticles remained consistent and high for both bovine serum albumin (BSA), a commonly used carrier or stabilizer for growth factors, and BDNF at a loading of 5 μg (Fig. 3c). Loadings higher than 5 μg with either BSA or BDNF did not increase EE.

The TEM images confirmed that the photocleavable nanoparticles had a uniform spherical morphology with a diameter range of 50–100 nm, which aligns with the size distribution observed in the pre-irradiation DLS measurements. The study also demonstrated the phototriggered disassembly and release of BDNF from the PEGOD-EA-LMB nanoparticles using an 808 nm NIR laser (Fig. 4a). The PCNs were disassembled at varying energy densities (0, 30, 60, and 90 J/cm^2) upon laser irradiation, as shown in the dynamic light scattering intensity distribution graphs (Fig. 4b), with a shift toward a

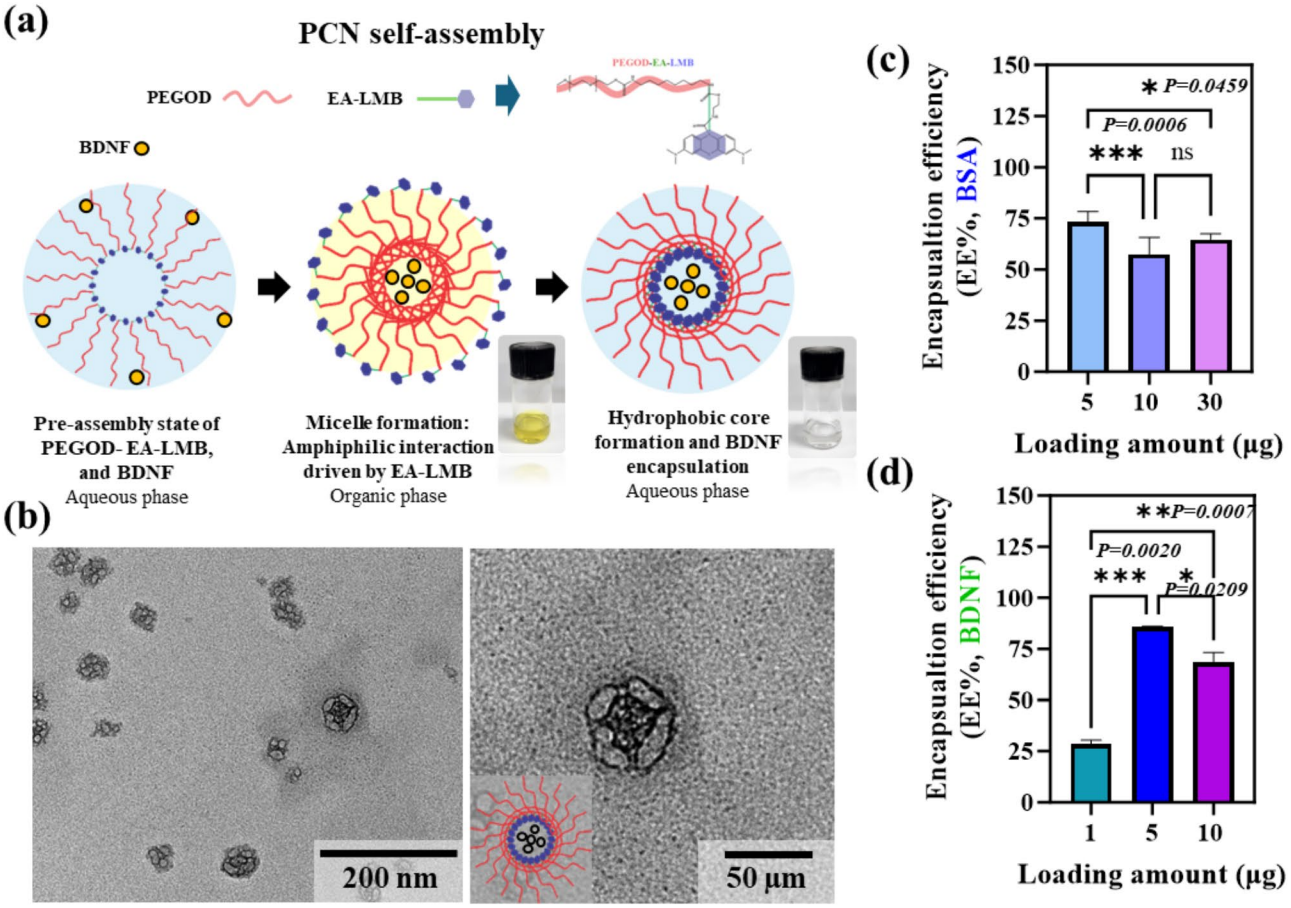

Fig. 3 Photocleavable nanoparticle (PCN) fabrication. (**a**) Schematic illustration of the self-assembly of polyethylene glycol octamethylene diamine–ethanolamine – leucomethylene blue (PEGOD-EA-LMB) polymer and encapsulation of brain-derived neurotropic factor (BDNF) in aqueous-–organic–aqueous solutions to form approximately 50 nm PCNs as observed by (**b**) transmission electron microscopy with hydrophobic LMB core and hydrophilic PEGOD tail. Loading amounts higher than 5 µg with either (**c**) bovine serum albumin or (**d**) BDNF did not increase encapsulation efficiency. The statistical significance of the data was analyzed using one-way ANOVA with Tukey's multiple comparisons test for each group ($n = 6$)

broader distribution of smaller-sized particles attributed to the formation of debris resulting from photocleavage (indicated by the asterisk). The mean particle diameter significantly decreased with no significant difference in the polydispersity index after laser irradiation, indicating homogenous cleavage of the nanoparticles (Fig. 4c). Higher laser irradiation energy density (90 J/cm2) formed larger agglomerated particles than in the other groups (Fig. 4d). The formed debris measured < 5 nm but > 2 nm for all laser-irradiated particles, in contrast to control or nonirradiated particles with debris ≤ 2 nm. The size distribution data suggest that laser irradiation at an energy density < 90 J/cm^2 could prevent the formation of agglomerated particles. The results indicate that PEGOD-EA-LMB nanoparticles can effectively disassemble and release BDNF using the 808 nm laser as a phototrigger.

The controlled release of BDNF from PCNs upon NIR laser irradiation occurs via a photocleavage mechanism intrinsic to the polymeric structure. Upon exposure to an 808 nm NIR laser, the LMB moiety undergoes oxidation, converting into its MB form through a reactive oxygen species (ROS)-mediated mechanism. This oxidative transition destabilizes the carbamate linkage within the PEGOD-EA-LMB structure, leading to bond cleavage. As a result, the polymer undergoes structural disassembly, triggering the controlled release of BDNF. Furthermore, ROS assays (S2) confirmed that NIR-triggered oxidation did not generate excessive ROS beyond physiological levels, further supporting this delivery system's non-cytotoxic and biocompatible nature.

BDNF is encapsulated through physical entrapment and weak intermolecular interactions. The self-assembly of PEGOD-EA-LMB forms nanoparticles with a hydrophobic LMB core and a hydrophilic PEGOD shell, ensuring a stable environment. Electrostatic interactions between BDNF's amine residues and the PEG hydroxyl groups further stabilize the encapsulated protein, preventing premature release. Upon laser activation, photocleavage disrupts these interactions, enabling controlled

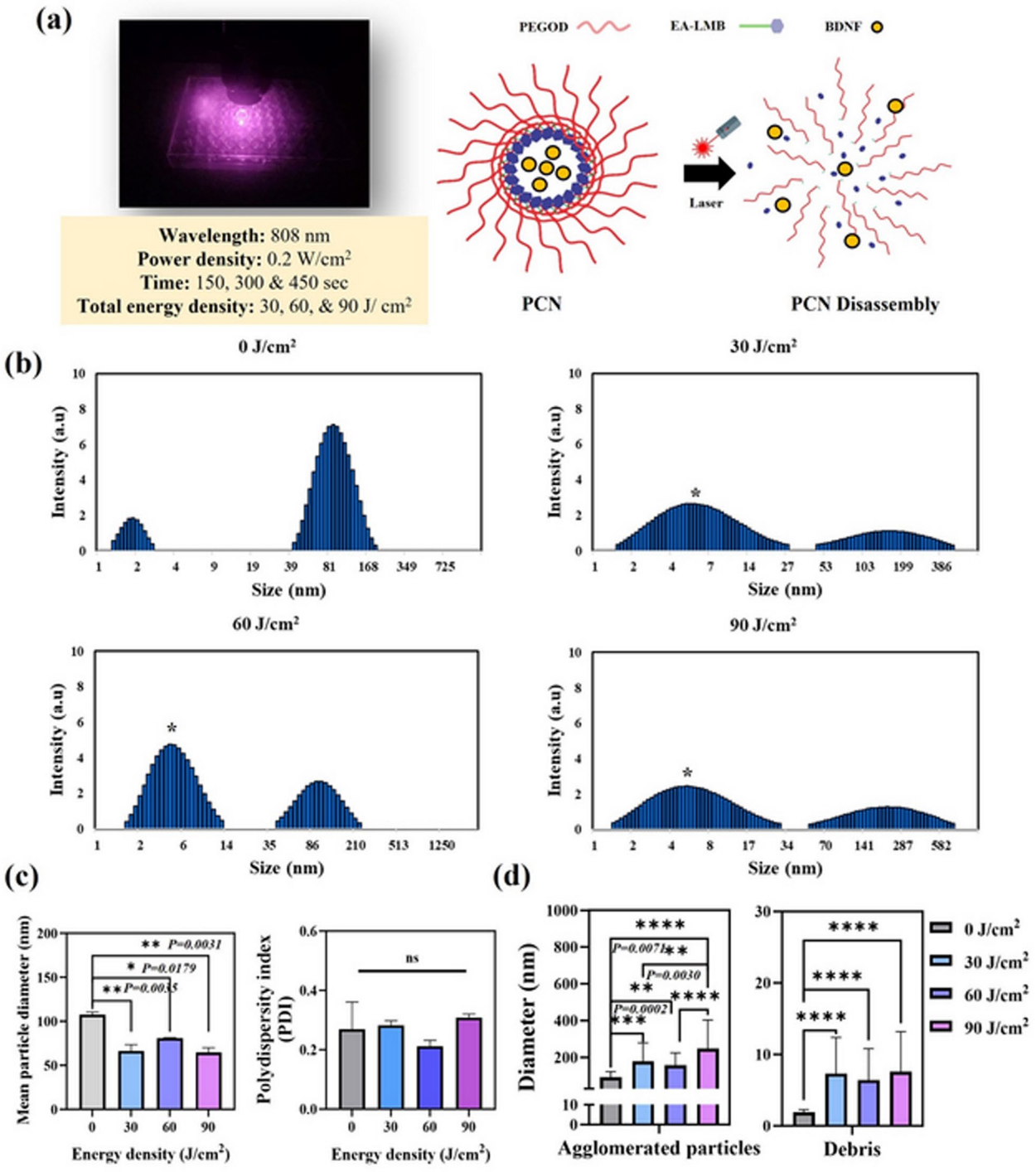

Fig. 4 Effect of laser irradiation on photocleavable nanoparticles (PCNs). (**a**) Schematic illustration of 808-nm laser irradiation and parameters used to disassemble nanoparticles for the phototriggered release of brain-derived neurotrophic factor. (**b**) Dynamic light scattering intensity distribution graphs show cleavage of nanoparticles upon laser irradiation at varying energy densities (0, 30, 60, and 90 J/cm^2), with a broader distribution of smaller-sized particles attributed to debris resulting in photocleavage. (**c**) Mean particle diameter significantly decreased (by half) after laser irradiation with no significant difference in the polydispersity index, indicative of homogenous cleavage. (**d**) However, at 90 J/cm^{2,} larger agglomerated particles formed significantly relative to the other groups. Formation of debris measuring < 5 nm but > 2 nm was observed for laser-irradiated particles. Groups were compared using one-way ANOVA with Tukey's multiple comparisons test (**** $P < 0.0001$)

and sustained BDNF release while preserving its structural integrity and biological activity.

Biocompatibility of the photocleavable nanoparticles

The results of the PCN cytotoxicity assay of human neural progenitor cells (hNPCs) indicated that concentrations of PCNs up to 900 µg/mL did not have any cytotoxic effects on hNPCs after 24 h in culture (Fig. 5a–b). Moreover, at 562 µg/mL, PCNs exhibited improved hNPC proliferation, likely due to an optimal balance of nanoparticle concentration, cellular uptake, and biological activity, enhancing cell adhesion and signaling. However, at higher concentrations (> 562 µg/mL), saturation effects or minor aggregation may have reduced bioavailability, leading to a plateau in proliferation. Similar trends are observed in nanoparticle-based delivery systems, where moderate concentrations promote cellular responses, but excessive amounts may diminish benefits. Future studies should further investigate nanoparticle-cell interactions and intracellular signaling pathways influencing proliferation. We also found that laser irradiation at energy densities of 30, 60, and 90 J/cm^2 did not affect the viability of hNPCs (Fig. 5c). Furthermore, the use of laser irradiation in combination with PCNs did not show any cytotoxic effects on hNPCs, as confirmed by the Cell Counting Kit-8 (CCK-8) assay and immunofluorescence imaging (Fig. 5d). The presence of PCNs on hNPCs was also confirmed by their fluorescence upon irradiation, which is attributed to the MB moiety that emits at 680–750 nm. This fluorescence also confirmed the successful photocleavage of PCNs, as emission was observable upon cleavage and conversion of LMB to MB. The findings of the cytotoxicity assay suggest that PCNs and laser irradiation are safe and biocompatible for human-derived and neural progenitor types of cells.

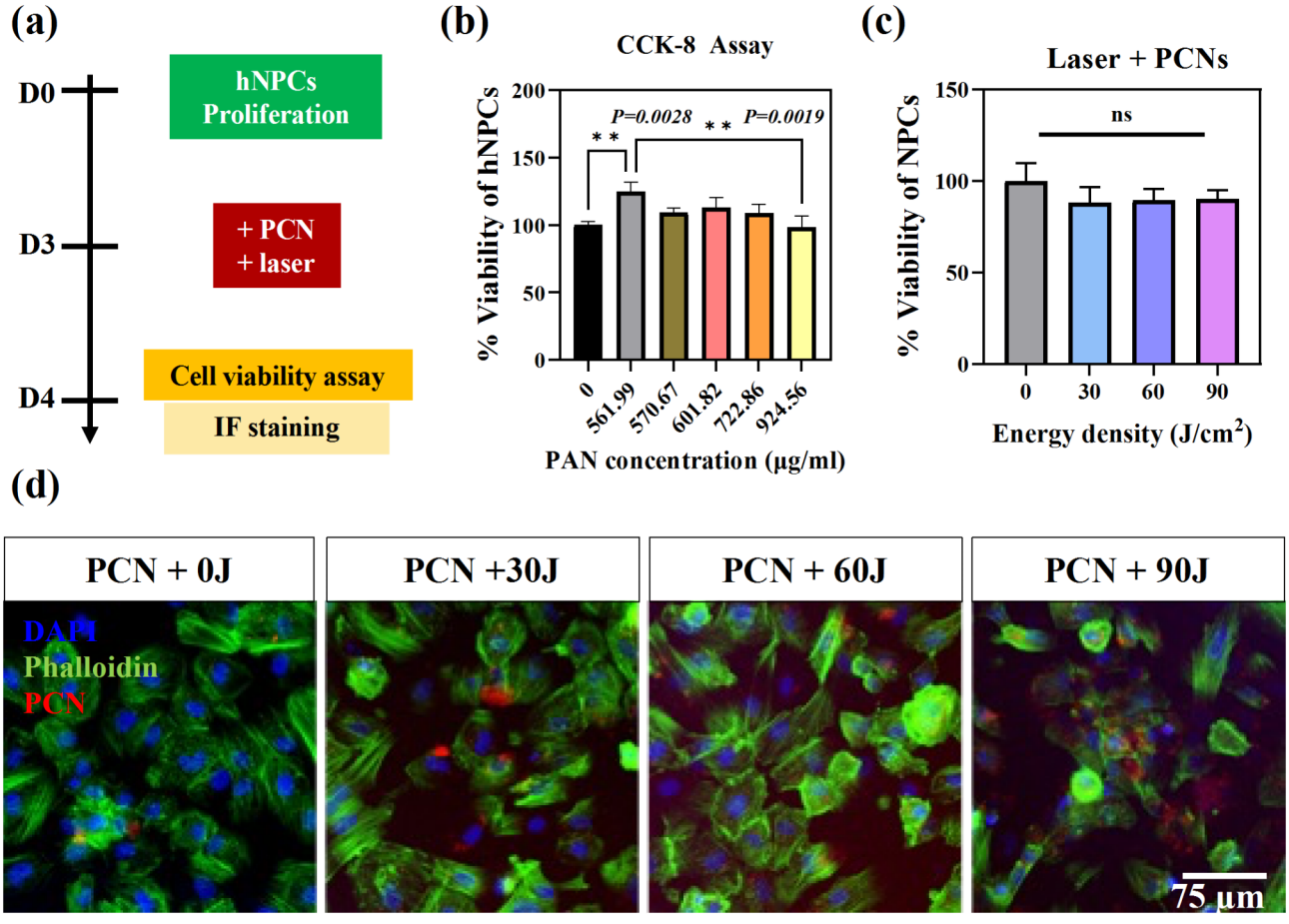

Fig. 5 Photocleavable nanoparticle (PCN) cytotoxicity assay in human neural progenitor cells (hNPCs). (**a**) hNPCs were grown in culture for 3 days prior to PCN or laser treatment, and viability assays were performed after 24 h. (**b**) Concentrations of PCN up to 900 µg/mL exhibited no cytotoxic effect on hNPCs. (**c**) Laser irradiation in combination with PCNs at energy densities of 30, 60, and 90 J/cm^2, did not affect hNPC viability after 24 h in culture, as determined by the CCK-8 assay. (**d**) Immunofluorescence images show the presence of PCNs in hNPCs, confirming that hNPCs remained viable after treatment and laser irradiation. Groups were compared using one-way ANOVA with Tukey's multiple comparisons test

Differentiation of hNPCs by photocleavable nanoparticles

In the study, 808-nm laser irradiation at different energy densities triggered the release of BDNF from PCNs in hNPCs (Fig. 6a). Irradiation at 60 J/cm^2 (89.15 ± 0.57%) resulted in BDNF release that was higher relative to 30 J/cm^2 (69.01 ± 2.86%) and control or no laser treatment (9.58 ± 1.99%), but was not significantly higher than 90 J/cm^2 (90.76 ± 1.94%). This result corresponds to the observed difference in growth and differentiation of hNPCs cultured for 7 days in neuronal differentiation medium (NDM) without the BDNF component and treated with PCNs and laser irradiation (Fig. 6b). The PCN concentration adjusted to release approximately 100 ng/mL of BDNF was designed to replace BDNF in the culture of hNPCs. PCN-releasing BDNF induced significant changes in the expression of the neural progenitor cell marker (Nestin) (Fig. 6c–d). Nestin expression was significantly higher for PCNs irradiated at 60 J/cm^2 than control (PCNs only) and PCNs irradiated at 90 J/cm^2, based on mean fluorescence intensity in confocal images processed using ImageJ software (NIH, Bethesda, MD, USA). Slight inhibition in the growth of hNPCs was observed for the 90 J/cm^2 laser treatment. Higher mean fluorescence intensity for PCNs and laser irradiation at 60 J/cm^2 was also observed for the mature neuronal cell marker (NeuN) relative to control (Fig. 6e–f). The results suggest that PCNs and phototriggered BDNF release at 60 J/cm^2 were able to support the growth and differentiation of hNPCs in culture.

Differentiation and characteristics of vestibular ganglion neuron (VGN) organoids

Vestibular ganglion organoids were developed to model vestibular neurons in animals. These organoids were generated from vestibular ganglion cells isolated from the cochlea of 1-day-old (P1) rat pups ($n = 22$) (Fig. 7a). Different culture methods were tested to optimize organoid formation. Initially, a mixture of Matrigel and single dissociated cells (1×10^5) was plated on an 18-mm cover glass. However, this approach led to incomplete aggregation (S3a-b). Next, a U-shaped 96-well plate was used to seed 3.5×10^3 dissociated cells, but the resulting cell clusters remained small (< 100 µm in diameter) (Figure S4a). Finally, plating a mixture of media and 3.5×10^4 cells produced clusters with an optimal diameter of approximately 300 µm (S4b). Once plated on flat cover glass, organoids exhibited neurite outgrowth, with continuous migration over time (S4c).

Among the various dissociated cell types, only a subset remained viable in proliferation media, gradually reducing total cell number (Fig. 7b, S5) [21–23]. We compared proliferation and neural differentiation media (NDM) (S6a) to determine the optimal culture conditions. By day 21 (D21), organoids cultured in NDM exhibited an early increase in NeuN-expressing cells and a decrease in NeuN- and GFP-negative cells (astrocyte marker) (S6b-d), indicating more efficient and accelerated neuronal differentiation. Notably, NDM contained BDNF and neurotrophin-3 (NT-3) neurotrophic factors, essential for neuronal differentiation and maturation. Based on these findings, NDM was selected for the later stages of organoid differentiation (Fig. 7c). For detailed methodology, refer to the Methods section.

VGN organoids cultured in NDM began expressing NeuN as early as day 3 (D3). The population of NeuN-positive cells significantly increased at D3 and D21 compared to D0 ($n = 6$; ** $P < 0.0001$), while Nestin-positive cells showed a decreasing trend over 21 days, though the reduction was not statistically significant ($n = 6$; $P > 0.05$) (S7b). These findings indicate the progressive differentiation of mature neurons in VGN organoids over time.

The morphology of NeuN- and Nestin-positive cells in primary VGNs (Fig. 7d) closely resembled that of VGN organoids at D21 (Fig. 7e). Serial epifluorescence analysis **(S7a, c)** also revealed the presence of glial cell markers. Astrocytes and microglia were identified using GFAP and Iba1, respectively. While the GFAP-positive cell population remained stable throughout the culture period, Iba1-positive cells showed a significant increase at D21 compared to D0 and D3 (*$n = 6$; $P < 0.05$). At D21, NeuN-positive cells (arrows) and GFP-positive cells (arrowheads) displayed distinct localization patterns (S6b).

To assess whether VGN organoids exhibit afferent neuron-specific characteristics, we analyzed calbindin and calretinin, well-established peripheral sensory nervous system (PNS) markers [24–26]. Additionally, Islet1, a key transcription factor in developing PNS neurons, was detected (S8) [27, 28]. Notably, NeuN and other neuronal markers were predominantly localized at the periphery of VGN organoids, likely due to their proximity to NDM. In contrast, Nestin expression at later differentiation stages was concentrated in the central region of the organoids (Fig. 7e), suggesting a spatial organization that reflects distinct neuronal maturation zones.

Verification of functional characteristics in VGN organoids

The functional properties of vestibular ganglion organoids were assessed using whole-cell patch clamp recordings. One day before the experiment, VGN organoids were transferred onto Poly-D-Lysine (PDL)-coated 18-mm round cover glass, allowing the organoids to attach to the coverslip (Fig. 8b). Due to their three-dimensional structure, the patch clamp procedure differed from conventional methods [29]. Instead, the electrode pipette was positioned first, and then the organoids were carefully brought into contact with the pipette.

For comparison, primary VGNs were also subjected to patch clamp recordings and exhibited Tuj1 expression, a

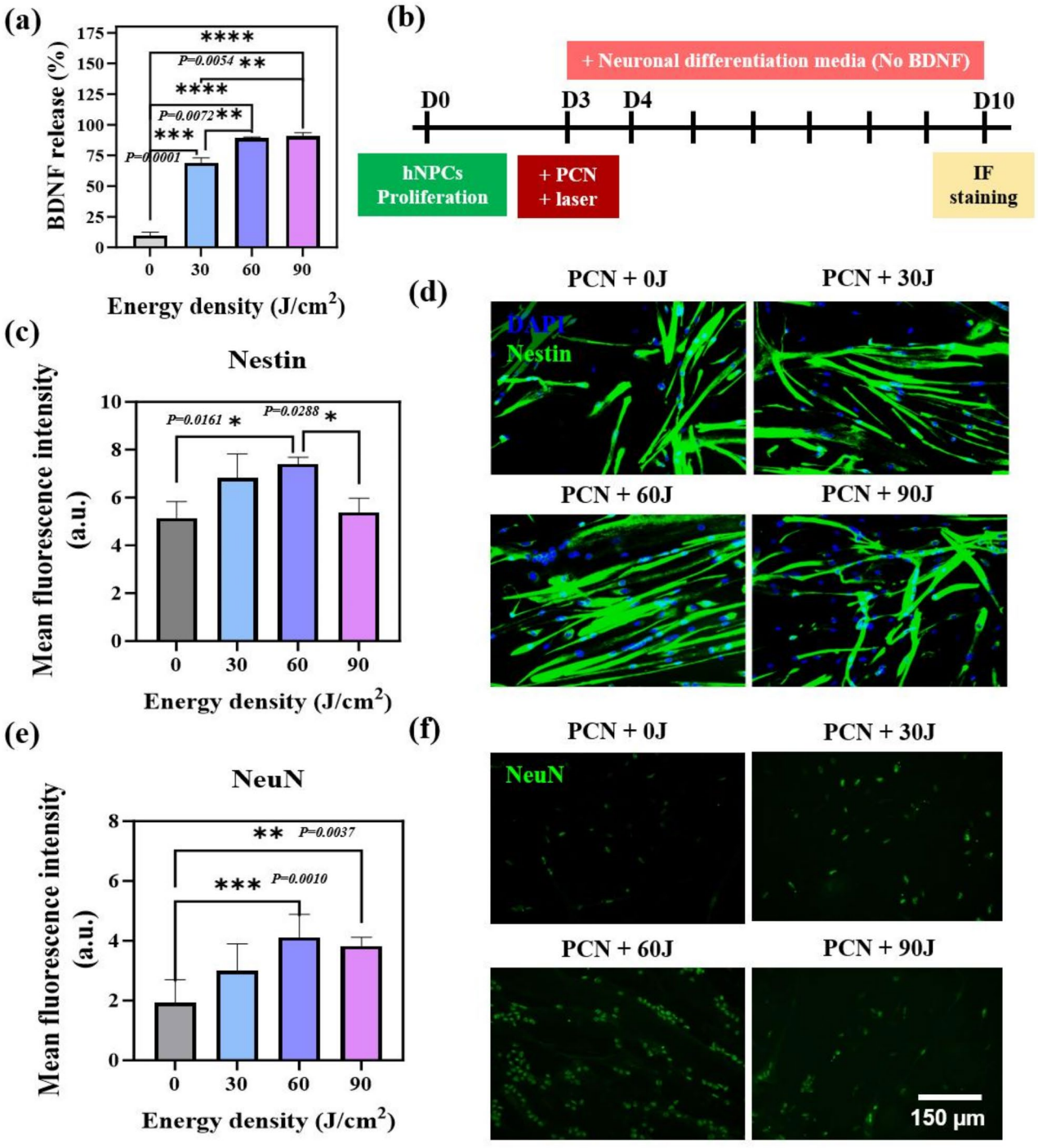

Fig. 6 Phototriggered release of brain-derived neurotrophic factor (BDNF) from photocleavable nanoparticles (PCNs) and its effects on the growth and maturation of human neural progenitor cells (hNPCs). (**a**) Amounts (%) of BDNF released in hNPCs at different energy densities (0, 30, 60, and 90 J/cm^2) after laser irradiation. Irradiation at 60 J/cm^2 (89.15%) showed BDNF release that was higher relative to 30 J/cm^2 (69.01%) but not significantly higher than 90 J/cm^2 (90.76%). (**b**) hNPCs were grown in culture for 3 days prior to PCN or laser treatment, and the medium was changed to neuronal differentiation medium (NDM) containing no BDNF. Maturation effects were determined after 7 days in NDM (D10). (**c**) The neural progenitor cell marker Nestin had significantly higher mean fluorescence intensity relative to PCN only and PCN + 90 J/cm^2, as assessed by immunohistochemical staining (**d**). (**e**) The corresponding immunofluorescence images also observed a higher mean fluorescence intensity with PCN + 60 J/cm^2 for the mature neuronal cell marker NeuN (f). Groups were compared using one-way ANOVA with Tukey's multiple comparisons test (**** $P < 0.0001$)

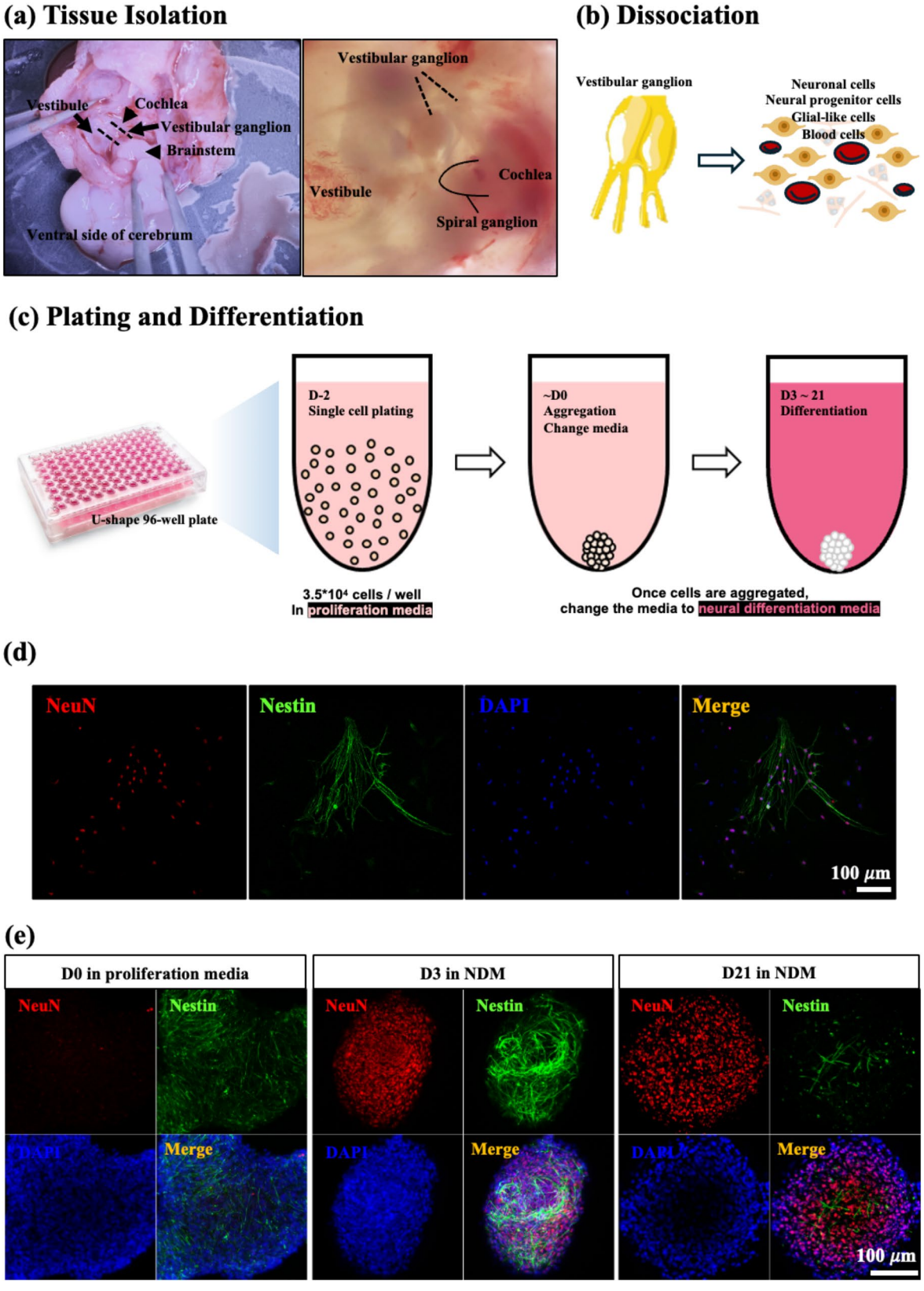

Fig. 7 (See legend on next page.)

(See figure on previous page.)

Fig. 7 Isolation of vestibular ganglion neurons (VGNs), three-dimensional (3D) organoids culture, and characterization. (**a**) Primary vestibular ganglion culture step 1: tissue isolation. Images of VGN isolation from P1 rat pups (dotted lines show vestibular ganglion utricle and saccule). (**b**) Primary vestibular ganglion culture step 2: Dissociation. TrypLE™ Express Enzyme dissociated vestibular ganglion into neuronal, neural progenitor, glial-like, and blood cells. (**c**) Primary vestibular ganglion culture step 3: Plating and differentiation. Every single cell is plated in a U-shape culture plate. 3D organoids were formed through aggregation by D0. Media was changed to neural differentiation media (NDM) on D0. As of D3, differentiation into VGN organoids started. (**d**) Representative immunofluorescence images show primary VGNs on D0. Most vestibular ganglion neurons are positive for neuron and neural stem cells, marked by neuronal cell markers, NeuN (red) and Nestin (green). (**e**) Representative confocal images of organoids show positive expression for neural stem cell marker Nestin and mature neuronal cell marker NeuN expressed 3 days after culture in NDM. Nestin expression decreased at day 21, while NeuN expression persisted

marker of peripheral sensory neurons [30] (S9). Sodium currents, indicative of neuronal excitability, were observed in patched cells from both primary VGNs and organoids (Fig. 8a-c). These signals disappeared after the replacement of extracellular sodium with N-methyl-d-glucamine (NMDG), confirming that the signals were sodium currents [31].

The I-V curve analysis showed a decrease in conductance after NMDG replacement, indicating Na^+ current blockade in both primary VGNs and organoids (Fig. 8d). These findings demonstrate that VGN organoids possess electrophysiological properties comparable to native vestibular neurons, confirming the successful generation of functional vestibular ganglion organoids.

Regenerative effect of PCNs with BDNF in a vestibular organoid disease model

Neuronal cell damage in vestibular organoids was induced using ouabain (03125; Sigma–Aldrich, St. Louis, MO, USA), a drug that causes neuronal damage. The organoids were also cultured in NDM without BDNF to determine PCNs' ability to successfully deliver BDNF and its regenerative effect in the disease model. The neuronal cell population in the organoids significantly decreased in the differentiation medium without BDNF, reflected in decreased expression of NeuN (Fig. 9a-b). Vestibular ganglion organoids in NDM without BDNF were treated with ouabain (0.2, 0.5, and 1 mM) on day 21, with cell viability assessment and immunofluorescence staining performed after 48 h (Fig. 9c). Cell viability (%) significantly and dose-dependently decreased with ouabain treatment (Fig. 9d). A concentration of 1 mM ouabain decreased cell viability by half and significantly decreased the expression of the mature neuronal cell marker NeuN (Fig. 9e), indicating that 1 mM of ouabain was the optimal concentration to induce vestibular neuronal cell damage.

Organoids were treated with 1 mM ouabain on day 21, and PCNs with laser treatment were administered after 24 h to assess the effects of PCNs with BDNF. Cell viability (%) and the expression of NeuN and Nestin were assessed 24 h after PCNs with laser treatment (Fig. 9f). Weak Nestin expression was observed after 1 mM ouabain treatment (Fig. 9g), which confirmed ouabain-induced damage. However, regeneration was confirmed with PCNs irradiated at 30 and 60 J/cm^2, when Nestin significantly improved or recovered. Nestin and NeuN expression did not significantly improve with PCNs and 90 J/cm^2 laser treatment, with a low number and significantly short length of Nestin-positive cells relative to other laser treatments (Fig. 9h). Therefore, laser irradiation at 30 and 60 J/cm^2 successfully released BDNF from PCNs into the damaged organoids, but the most significant regenerative effect was observed with 60 J/cm^2 laser treatment. In contrast, 90 J/cm^2 did not show regenerative effects in damaged organoids. Overall, the results indicate that the PCNs in this study could be a powerful tool to treat inner ear dysfunction, particularly vestibular neuropathy, when used as a delivery system for BDNF.

Discussion

Light source and irradiation parameters

Laser stands for "light amplification by stimulated emission of radiation." A laser emits coherent light of a single wavelength [32], while light-emitting diodes (LEDs) produce noncoherent light across a range of wavelengths [33]. Lasers are typically more focused, intense, and directional, while LEDs are more diffuse and less intense. Lasers are commonly used in applications requiring precision and focus, such as laser cutting, laser surgery, barcode scanners, and optical communications (e.g., fiber optics). Their coherent light allows for tight focusing over long distances. On the other hand, LEDs are versatile and used in various applications, including lighting (bulbs, displays), indicators, remote controls, and automotive lighting. They provide energy-efficient illumination and are often preferred for general lighting due to their lower cost and broader range of colors [34]. The inner ear is a relatively small organ, and the delivery route is mostly through the tympanic membrane. Therefore, light energy delivery should be highly focused as used in the experiment. As mentioned, the wavelength is crucial for inner ear delivery. Previous studies [20, 35] and our data (S10) revealed that the penetration depth of NIR light is necessary for deeply located target organs with power density kept within 200 mW to prevent damage to surrounding tissue. Currently, most light-activated drug releases adopt low wavelength parameters, which have a relatively low penetration rate. Higher penetration is necessary for the use of controlled drug delivery to anatomically deeply

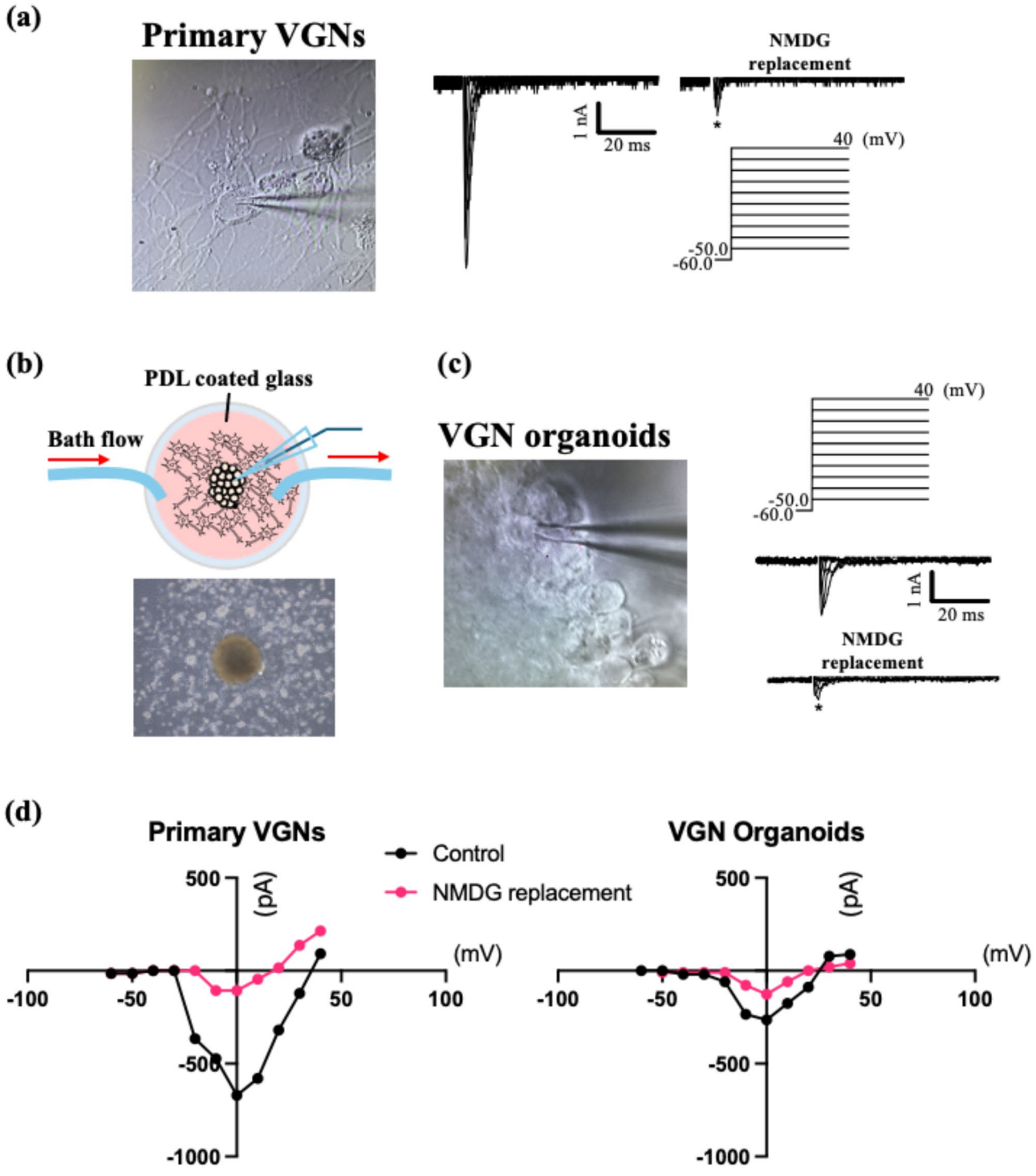

Fig. 8 Functional assessment of primary VGNs and organoids (**a**) and (**c**) Sodium currents were generated by patched cells from the differentiated primary VGNs culture and organoids, indicative of depolarization and activity. Depolarizing pulses induced inward currents, which were blocked almost completely in a low-sodium condition (*140 mM NMDG replacement). (**b**) A scheme of whole cell patch clamp on the VGN organoids. Organoid is on the Poly-D-Lysine (PDL)-coated 18-mm cover glass to avoid being washed away by bath flow. (**d**) I-V curve of both primary VGNs and organoids shows Na + conductance before and after NMDG replacement, showing a comparable conductance pattern

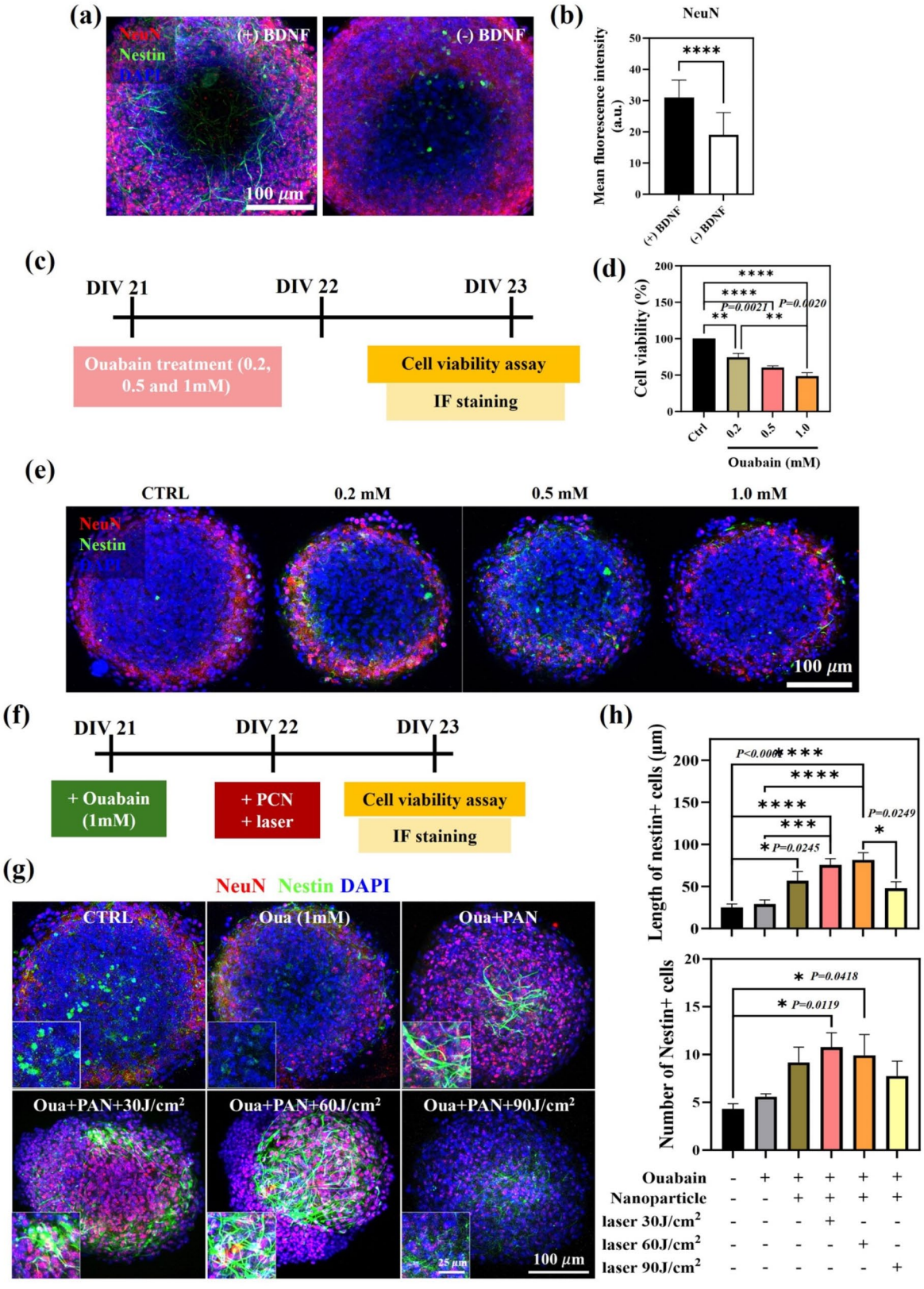

Fig. 9 (See legend on next page.)

(See figure on previous page.)

Fig. 9 Effects of laser and photocleavable nanoparticles (PCNs) loaded with brain-derived neurotrophic factor (BDNF) on ouabain-induced neuronal damage in vestibular ganglion neuron (VGN) organoids. (**a**) Confocal images of VGN organoids cultured in a differentiation medium for 21 days showed a decrease in Nestin expression with neurotrophic factor NT-3 without BDNF. (**b**) The mature neuronal cell marker NeuN also decreased without BDNF in the medium, as shown in the mean fluorescence intensity graph. (**c**) VGN organoids ouabain treatment concentration and cytotoxicity evaluation schedule. (**d**) Immunofluorescence staining revealed a decrease in NeuN expression with increasing ouabain concentration, with a significant decrease in cell viability. (**e**) Ouabain induced damage in VGN organoids in a dose-dependent manner, with a 0–5% decrease in cell viability observed with 1 mM after 24 h. (**f**) An experimental schedule of PCNs and laser treatment of VGN organoids damaged by ouabain were used. (**g**) Immunofluorescence images after ouabain, PCN, and laser treatments with a corresponding assessment of (**h**) the length and number of Nestin-positive cells. Few Nestin-expressed cells were observed in the control or ouabain group, while the PCN- and the number and length of Nestin-positive cells were markedly increased in the laser-treated groups, except at the energy level of 90 J/cm^2. Groups were compared using one-way ANOVA with Tukey's multiple comparisons test (**** $P < 0.0001$)

located target organs such as the inner ear. The laser's NIR wavelength shows fair energy penetration, which could be used as a non-invasive (without further surgical procedures to deliver light energy to the target organ) trigger for BDNF release.

BDNF load and laser energy

The optimum amount of BDNF loading via the self-assembly in the PCNs was determined. A higher amount of BDNF (> 5 μg) could not be trapped more efficiently within the PEG network upon intercalation during the organic solvent dissolution due to repulsive forces between amine residues in BDNF and hydroxyl groups in the PEG backbone. The entrapment of BDNF within the intercalated PEG and LMB core prevents premature release in an aqueous solution. However, long-term stability remains to be determined. BDNF is released by photocleavage and the correlation between nanoparticle disassembly and cellular viability provides key insights into the optimization of energy density for effective BDNF delivery. The study determined that an energy density of 60 J/cm² is optimal, as it maximizes BDNF release while maintaining uniform nanoparticle cleavage and minimizing the formation of large aggregates. Higher energy densities, such as 90 J/cm², led to excessive agglomeration, potentially reducing BDNF bioavailability and inducing cellular stress. Findings demonstrated that BDNF release triggered at 60 J/cm² significantly enhanced neuronal differentiation, as observed by increased Nestin and NeuN expression. Conversely, at 90 J/cm², reduced differentiation and viability were evident, aligning with the aggregation effects observed. These results highlight that excessive energy input disrupts nanoparticle stability and negatively impacts cellular response, underscoring the importance of selecting an optimal energy density for therapeutic applications. Cytotoxicity assays confirmed that 60 J/cm² effectively supports neural progenitor differentiation without significant adverse effects, ensuring that the selected energy density delivers BDNF while preserving cellular health. Hence, this parameter was used in the organoid disease model, wherein BDNF was omitted from the differentiation protocol and replaced by PCNs as the source of BDNF. The optimized laser energy density supported Nestin expression in vestibular organoids and facilitated significant neuronal recovery, demonstrating that laser-triggered BDNF release effectively promotes neuronal regeneration without causing adverse effects. This controlled release system was designed to mimic physiological BDNF levels, thereby avoiding overstimulation or desensitization of neurotrophic signaling pathways, a crucial factor for maintaining long-term therapeutic efficacy. These results underscore the importance of precise energy calibration to maximize therapeutic benefits while preserving cellular health. Future studies should focus on further optimizing NIR dosage, evaluating the long-term impacts of sustained BDNF release, and investigating potential adaptive cellular responses to repeated laser treatments, particularly in vivo, to advance the therapeutic potential of this approach.

Previous studies have demonstrated that similar photocleavable systems maintain prolonged stability in aqueous environments, preventing premature drug leakage and preserving therapeutic integrity until triggered by light [16, 39]. These findings suggest that repeated activation and sustained drug release are feasible, supporting the clinical applicability of this approach. Future studies will further assess the long-term stability and efficiency of repeated NIR-induced release in our system.

Impact of vestibular ganglion neuron organoids

The possibility of robust regeneration of a vestibular nucleus that connects to a vestibular ganglion has been proposed [36]. In addition, the possibility of vestibular ganglion regeneration has been reported [37], and a vestibular ganglion neuron isolation technique has been established [38]. However, very few studies have reported successful regeneration of functional three-dimensional (3D) vestibular ganglion structures. We dissociated the cells from the vestibular ganglion and used a technique to differentiate the vestibular ganglion neuron from neural progenitor cells. Again, this confirmed the ability to regenerate or differentiate from progenitor cells. On differentiation day 0, there were no mature neurons, but after 3 days of culture, numerous mature neurons were observed, which indicated that these cells were differentiated from neural progenitor or neural stem cells. With the current disease model, we can differentially evaluate

the target cell for individual diseases and therapeutic agents. Furthermore, since the robust innate neural connectivity of a vestibular neuron has been revealed [37], evaluation of possible methods to reestablish the connection between a vestibular ganglion and a vestibular nucleus might be possible.

In the present study, we used the vestibular neuron organoid as a disease model instead of an animal model. There are reports of an animal model for unilateral vestibulopathy [39, 40], but mimicking human conditions was challenging. There are several reasons for this. First, the rodent vestibular system has a better recovery capacity compared with clinical conditions. After unilateral damage of vestibular afferent neurons, the majority of rodent animal models displayed almost complete recovery of balance [39]; this differs from the clinical condition, in which balance disabilities remain [41–43]. In addition, it is widely believed that 'vestibular neuritis' is a specific disease of vestibular neurons [44, 45]. However, isolated damage to a neuron is not feasible. Evaluations using behavioral tests involve numerous other areas of the brain. Thus, evaluating a pharmacologic agent in relation to this specific target is challenging. Organoids are cultured based on pluripotent or multipotent cells and form 3D structures, such as target organs, via self-renewal and self-organization. They serve as research tools as they are composed of multiple cells capable of performing target functions [46]. Since they can resemble the structures and functions of organs, they have been adopted as tools for modeling diseases, drug screening, and regenerative research [47]. In the present study, we developed an electrophysiologically confirmed organoid that imitated vestibular neurons as a model to confirm the effect of PCNs. Although it is difficult to evaluate some characteristics such as response to injury, the organoid shows comparable regeneration capacity to primary vestibular organoid (Fig. S7: organoid; primary culture data not shown). This organoid can confirm the effect of PCNs on vestibular neurons as regenerative therapy using BDNF; we are currently elaborating on this finding. Attaching a homing particle to target inner ear neurons could also be applied to spiral ganglions for cochlear implantation, with encapsulation of cells such as neural progenitor cells. We envisage multiple applications for many other neural diseases that affect deep-lying structures and require a controlled release to reduce unwanted effects.

Mechanistic insights into regeneration

BDNF's effects on vestibular neuron regeneration involve a network of interrelated signaling pathways that collectively enhance neuron survival, axon regrowth, synaptic plasticity, and functional recovery. BDNF-mediated PI3K/Akt and MAPK/ERK signaling enhance axon elongation and branching [48]. PLCγ/PKC activation supports neurotransmission recovery. PI3K/Akt and JAK/STAT protect against apoptosis and oxidative stress [49]. ERK1/2 promotes long-term changes in vestibular circuitry, which is crucial for restoring balance function [48]. These multiple roles of BDNF might be helpful for the treatment of hidden vestibulopathy [50], which is presumed to be related to the synaptic connection between the sensory cell and the vestibular nerve. So far, the clinical impact, such as related symptomatic correlation, has not been established yet. Nevertheless, BDNF could be optimal for treating these neural pathologies, including synaptopathy.

Clinical implication

These promising results in the organoid model in the present study indicate that selective and timely treatment of BDNF is possible without damaging the surrounding structure. Since BDNF is a growth factor that could lead to the growth of nervous structures, treatment could lead to unwanted growth of neurons, leading to hyperexcitation of neuronal response in the vestibular system or other surrounding systems. With this controlled photo-activated release, more detailed and tailored, less invasive treatment would be possible and greatly enhance patients' quality of life with uncompensated vestibulopathy.

Materials and methods

Synthesis and characterization of the photocleavable polymer

The NIR-photocleavable polymer used in this study (PEGOD-EA-LMB) was synthesized based on a previously described protocol [51] with some modifications. In brief, 50 g of poly(ethylene glycol) methyl ether (mPEG; 5,000 Da; 81323; Sigma–Aldrich) was dissolved in 100 mL of toluene (8541 – 4100; Daejung; Siheung, South Korea) and subjected to azeotropic distillation until the volume was reduced to about 20 mL of visibly clear solution. Separately, 20 mmol of 4-nitrophenyl chloroformate (160210; Sigma–Aldrich) and 20 mmol of triethylamine (85556 – 4400; Daejung) were dissolved in 10 mL of dichloromethane (DCM; Samchun Chemicals, Seoul, South Korea) and added dropwise to the mPEG solution, which was stirred overnight at room temperature (RT). The mixture was slowly added to diethyl ether (4025–4400; Daejung) on ice with continuous stirring to precipitate the product. The precipitated product was purified by dissolution–precipitation with DCM and diethyl ether and recrystallized in ethyl acetate (4016 – 1100; Daejung). The PEG-nitrophenyl intermediary product was vacuum-dried. Next, 5 mmol of PEG-nitrophenyl was dissolved in 10 mL of DCM and added dropwise to a solution of octamethylene diamine (20 mmol) dissolved first in methanol (5558 – 4400; Daejung) and then in DCM. Triethylamine

(2 mmol) in DCM was added (250 µL) to the solution and stirred overnight. The reaction mixture was precipitated in diethyl ether with dissolution–precipitation and recrystallization steps similar to the first intermediary product, PEG-nitrophenyl. The resulting product was PEGOD. The product was vacuum-dried and stored under reduced pressure prior to use.

Modified 10-N-carbamoyl MB was synthesized according to previously described protocols with some modifications [52] and conjugated to the synthesized PEGOD. The modified product LMB was dissolved in DCM (5 mmol) and added dropwise to a solution of PEGOD in DCM (2 mmol). Triethylamine (2 mmol) in DCM was added (250 µL) to the solution. The reaction was run overnight and precipitated, purified, and recrystallized, following protocols similar to those of the intermediary products. The resulting product, PEGOD-EA-LMB, was vacuum-dried and stored in the dark under reduced pressure.

The chemical structure of the synthesized PEGOD-EA-LMB was characterized by ^{1}H NMR (sample dissolved in $CDCl_3$, δ ppm: 7.24) using a Bruker AVANCE 600 (Bruker, Billerica, MA, USA) instrument. The molecular weight was calculated based on the ratio of end-group protons to polymer chain protons. FT- IR (6100 type A; JASCO, Tokyo, Japan) was also performed to confirm the synthesized polymer. A potassium bromide (KBr) disk containing 1.0 wt% of the sample was analyzed in the range of 4,000–400 cm^{-1} at a resolution of 4 cm^{-1} with 32 cumulative scans.

Fabrication of PCNs

Photocleavable nanoparticles were formed via the self-assembly mechanism in aqueous–organic–aqueous solutions followed by drying steps. First, 30 mg of PEGOD-EA-LMB polymer was dissolved in Dulbecco's phosphate-buffered saline (DPBS; 20-031-CV; Corning, Jiangsu, China) containing different concentrations of either BSA (BioShop, Burlington, Canada: 5, 10, and 30 µg) or BDNF (788902; BioLegend, San Diego, CA, USA: 1, 5, and 10 µg), and freeze-dried. The powder was resuspended in ethyl acetate and vacuum-dried. The dried powder was reconstituted in PBS for subsequent analysis. Samples were kept in the dark at 4 °C to maintain stability. The generated nanoparticles were morphologically assessed by TEM (JEM 1400; JEOL, Tokyo, Japan). The % EE for BSA and BDNF in nanoparticles was calculated as (total BDNF added– free BDNF)/total BDNF added.

Light treatment of PCNs

A commercially available laser with a wavelength of 808 nm and frequency of 47–63 Hz (PSU-III-LED; CNI Laser, Changchun, China) was used according to the manufacturer's instructions. UV (254 nm) exposure was performed using CL-1000 UV Crosslinker (UVP, Upland, CA, USA). Dosimetry was performed to determine laser settings before conducting laser treatment using a power meter probe and measuring the power output of the laser handpiece at a distance of 3.0 cm from the bottom of the plate (average penetration rate of 17% in a 4-week-old C57B6 mouse purchased from NARA Biotech (Seoul, South Korea)). The laser setting was adjusted to achieve a power density of 200 mW/cm^2. Each laser shot was adjusted based on the irradiation time (150, 300, and 450 s) to achieve the specified energy densities (30, 60, and 90 J/cm^2, respectively). The effect of laser treatment on the size of the PCNs was evaluated by dynamic light scattering using a zeta potential and particle size analyzer (ELSZ-2000; Otsuka Electronics, Osaka, Japan).

Evaluation of cytotoxic effects of PCNs and laser treatment on hNPCs

hNPCs (ACS-5004; ATCC, Manassas, VA, USA) were used to determine the cytotoxicity of PCNs in culture. To culture hNPCs, plates were coated with 1% cellular basement membrane (ATCC) for 1 h at RT before seeding. For the cytotoxicity evaluation of the PCNs, hNPCs were seeded in coated 96-well plates with a cell concentration of 2×10^4 cells/mL, cultured in recommended commercial hNPC growth medium (ACS-3003; ATCC), and maintained inside an incubator at 37 °C and 5% CO_2. The hNPCs were grown and allowed to proliferate for 3 days prior to treatment.

Different concentrations of PCNs (500–1,000 µg/mL) were prepared by suspending the particles in the hNPC growth medium. Medium from the hNPCs grown in 96-well plates was removed, and PCNs were added to each well (100 µL) containing hNPCs kept for 24 h inside the incubator at 37 °C and 5% CO_2 before cytotoxicity assay. Cytotoxicity assay was performed using CCK-8/EZ-Cytox assay (DoGenBio, Seoul, South Korea). The assay detects viable cells based on water-soluble tetrazolium salt (WST-8) reduced by dehydrogenase activities, giving a yellow formazan dye soluble in the tissue culture medium. The solution was mixed at a ratio of 1:9 with fresh medium and incubated for 4 h inside the incubator at 37 °C and 5% CO_2. Optical densities were obtained at 450 nm using a microplate reader (Infinite 200 PRO; Tecan, Grödig, Austria). Triplicate readings were obtained from at least three individual culture and treatment batches. The data are reported as mean ± standard deviation. The same treatment schedule and protocols were followed for the determination of the potential cytotoxic effects of laser-only treatment and PCNs (500 µg/mL) at different energy densities (30, 60, and 90 J/cm^2) in hNPCs for CCK-8 viability assay. PCNs suspended in PBS were centrifuged and resuspended in an

hNPC growth medium. The PCNs were sonicated prior to use to remove agglomeration. Additional immunofluorescence staining was performed for PCNs with laser treatment. The hNPCs were stained with Alexa Fluor™ 488 Phalloidin (A12379; Invitrogen, Carlsbad, CA, USA), which selectively stains the filamentous actin (F-actin) of cells, with 4′,6-diamidino-2-phenylindole (DAPI; 5087410001; Sigma–Aldrich) used for nuclei staining. The samples were observed under a fluorescence microscope (EVOS™ M7000 Imaging System; Invitrogen, Darmstadt, Germany).

Effects of laser treatment and PCNs on hNPC differentiation

The amount of BDNF released (%) from PCNs upon irradiation at different energy densities (0, 30, 60, and 90 J/cm^2) was determined using a Human BDNF ELISA Kit (ab212166; Abcam, Eugene, OR, USA) following the manufacturer's protocol. The amount of PCNs needed to deliver approximately 100 ng of BDNF onto the cultured hNPCs during neuronal differentiation was calculated.

First, hNPCs in growth medium cultured for 3 days were treated with PCNs and laser irradiation. After treatment, the growth medium was changed to NDM without BDNF consisting of basal Dulbecco's modified Eagle's medium (DMEM)/Ham's F12 (10-090-CV; Corning, Corning, NY, USA), 1× N2 Supplement (17502-048; Gibco; ThermoFisher Scientific, Waltham, MA, USA), 2× B27 Supplement (17504-044; Gibco), 1% penicillin/streptomycin (30-2300; ATCC), 1,000 U/mL leukemia inhibitory factor (LIF; ESG1107; Millipore, St. Louis, MO, USA), and 10 ng/mL NT-3 (712102; BioLegend). BDNF was omitted from the medium to assess the effects on differentiation of BDNF released from PCNs alone. The hNPCs were kept for 7 days in culture and fixed for immunofluorescence staining. Images were acquired using the fluorescence microscope. The mean fluorescence intensity via obtained using ImageJ analysis of three batches of samples with an average of six images.

Primary vestibular ganglion culture

Vestibular ganglion isolation

Postnatal day 1 pup (P1; $n = 22$) of Sprague–Dawley rats were used in this study. We rinsed the pups' head and neck parts with 70% ethanol and decapitated using surgical scissors. After opening the skin, using the tips of Iris scissors, an incision was made along the midline of the skull, starting from the brainstem area. The cerebrum part was lifted toward the brainstem to expose the ventral side of the brain by flipping it over using curved forceps. At this point, we can identify two nerve bundles connecting the brainstem and the inner ear (Fig. 7a). The end of the nerve bundles of the brainstem was cut using micro scissors, and then the inner ear was extracted in cold 1x HBSS (14025-092; Gibco). We can distinguish the vestibular ganglion on the extracted inner ear (Fig. 7a). The vestibular ganglions were isolated from the inner ear using fine forceps and collected in a 1.5 ml tube containing 1x HBSS (Gibco) [28].

Vestibular ganglion dissociation

The vestibular ganglions were transferred to another 1.5 ml tube containing prewarmed TrypLE™ Express Enzyme (12604-013; Gibco) and incubated in a 37 °C water bath for 20 min. After incubation, TrypLE™ Express Enzyme was removed, and the ganglion were washed using 1x HBSS three times. The ganglion was dissociated using pipette of 1000, 200, and 10 μl. After dissociation, they were separated as single cells using 40 μm cell strainer (352340; Corning). Cell count was performed using Hematocytometer and Trypan Blue (15250-061; Gibco).

Vestibular ganglion organoids plating and differentiation

After dissociation, 3.5×10^4 of cells were seeded into a PrimeSurface 96 M 3D cell culture plate (MS9096UZ; S-BIO, NH, Hudson, USA). First two days of the culture are considered as -2 and – 1 day, which is for proliferation under proliferation media. The proliferation medium consisted of neurobasal medium (21103-049; Gibco) supplemented with 2% of B27 (17504-044; Gibco), 1% of GlutaMAX (35050-061; Gibco), and 5,000 U/mL penicillin/5,000 µg/mL streptomycin (Corning) (Table 1). In the proliferation media, cells begin to aggregate, and at this time, cells other than ganglia cells are degenerated due to the characteristic of proliferation media which allows the limited survival of the other cells [21–23]. In the primary VGNs culture, decreased number of cells are also observed at D0 compared to D-2 (S5). Once confluence was achieved or sufficient cells were aggregated, organoids were transferred to new 3D cell culture plate containing neural differentiation media (NDM). The NDM consisted of DMEM/Ham's F12 (Corning) supplemented with 2% of B27 (Gibco), and 1% each of GlutaMAX (Gibco) and N2 (17502-048; Gibco). Additionally, 10 ng/mL each of BDNF (BioLegend) and NT-3 (BioLegend) were added for differentiation (Table 2). Medium

Table 1 Media composition of proliferation media

Proliferation Media	
	Add (50 ml)
Neurobasal	48 ml
2% B27 supplement	1 ml
1% Glutamax	0.5 ml
1% Penicillin / Streptomycin	0.5 ml

Table 2 Media composition of neural differentiation media

Neural Differentiation Media (NDM)	
	Add (50 ml)
DMEM/Ham's F12	47.9 ml
2% B27 supplement	1 ml
1% Glutamax	0.5 ml
1% N2 supplement	0.5 ml
10ng/ml of BDNF (10ug/ml)	50 μl
10ng/ml of NT3 (10ug/ml)	50 μl

change and differential interference contrast imaging was performed every 3 days. Primary VGNs culture was also performed. 9×10^4 of cells were seeded into 12-well plate including proliferation media with 18-mm cover glass coated by 0.5 μg/ml of Poly-D-Lysine (A3890401; Gibco).

Cells were fixed on D0, D3, and D21 for immunohistochemical evaluation to confirm the characteristics and differentiation of vestibular ganglion culture. Whole-cell patch clamp and vestibular organoid disease modeling were performed on D21, which was considered the complete differentiation stage in our culture system. Cells were grown in NDM without BDNF and treated with 1 mM ouabain (Sigma–Aldrich) for vestibular organoid disease modeling.

Immunofluorescence staining

Cells were fixed in 100% methanol or 4% paraformaldehyde and permeabilized with 0.3% or 0.1% Triton X-100 (T8787; Sigma–Aldrich) in 1 × PBS. After blocking in 10% or 3% BSA (ALB001; BioShop), cells were treated with anti-Nestin (NBP1-92717; Novus Biologicals, Centennial, CO, USA), anti-neuronal nuclei (NeuN; ab177487; Abcam), anti-glial fibrillary acidic protein (GFAP; MAB360; EMD Millipore, Burlington, MA, USA), ionized calcium-binding adapter molecule1 (Iba1; ab178846; Abcam), anti-calbindin (ab1778; Abcam), calretinin (MAB1568; EMD Millipore), anti-insulin gene enhancer protein (islet1; ab20670; Abcam), and class III β-tubulin (Tuj1; 801201; BioLegend) and incubated overnight at 4 °C. One day after primary antibody treatment, cells were washed with 1 × PBS, incubated with Alexa Fluor 488 and 555, and goat anti-mouse or -rabbit conjugated secondary antibodies (Invitrogen) for 1.5 h at RT. Then, cells were washed three times with 1× PBS for 5 min each and mounted with DAPI-containing VECTASHIELD anti-fade mounting medium (H-1200; Vector Laboratories, Burlingame, CA, USA). Single-cavity microscope slides (76×26 mm^2 with ground edges; 1042001; Heinz Herenz, Hamburg, Germany) were used to mount vestibular ganglion organoids. Cells were observed with a confocal microscope (FV31-S; Olympus, Tokyo, Japan) to obtain representative images. The Nestin- and NeuN-positive cells were manually counted, and Nestin lengths were measured using ImageJ. The length of Nestin-expressing cells was obtained by measuring from the soma to the edge of Nestin-positive cells. Cell population analysis was carried out in more than four randomly selected regions of interest from three batches of samples.

Electrophysiology

Whole-cell currents were recorded from cultured vestibular ganglion cells differentiated for up to 21 days (D21). All experiments were performed at RT using an EPC-8 amplifier (HEKA, Lambrecht, Germany). Electrodes (3–5 MΩ) were filled with a solution containing Cs-methanesulfonate (140 mM; Sigma–Aldrich), EGTA (0.1 mM; Merck, Darmstadt, Germany), HEPES (20 mM; Gibco), Mg-ATP (1 mM; Sigma–Aldrich), Na_2GTP (1 mM; Merck), sucrose (10 mM; Sigma–Aldrich), and TEA-Cl (10 mM; Tocris Bioscience, Toronto, Canada). The internal solution was titrated with CsOH (Merck). The data were filtered at 5 kHz (EPC-8; HEKA), digitized at 10 kHz, and stored in the computer via WinWCP software (ver. 5.7.0; University of Strathclyde, Glasgow, UK) for offline analysis. The stored data were analyzed using Clampfit 11.2 (Molecular Devices, San Jose, CA, USA).

More detailed information related to organoids' whole cell patch clamp technique was described in results 2.7.

Statistical analysis

Data were analyzed using GraphPad Prism version 10.1.2 (GraphPad Software Inc., San Diego, CA, USA) and one-way ANOVA with Tukey's post hoc test used for multiple comparisons unless stated otherwise. P-values < 0.05 were considered significant.

Conclusion

This study presents a novel approach to treating vestibular neuropathies using NIR laser-induced PCNs with BDNF. The synthesized amphiphilic polymer, PEGOD-EA-LMB, demonstrated successful self-assembly into nanoparticles capable of encapsulating BDNF, offering a promising delivery system for growth factors in the inner ear. The photocleavable nature of these nanoparticles enabled the precise and controlled release of BDNF upon NIR laser irradiation that significantly influenced the growth and differentiation of hNPCs, indicating the efficacy of this delivery system in promoting neural development. Moreover, the study successfully generated vestibular ganglion organoids that closely mimic vestibular neurons, providing a valuable model for vestibular

neuropathies. The regenerative effects of PCNs loaded with BDNF were successfully evaluated in a vestibular organoid disease model induced by ouabain. The results demonstrated that PCNs, when irradiated with NIR laser, which is non-cytotoxic at appropriate energy densities, effectively delivered BDNF and promoted regeneration of damaged vestibular neurons.

Overall, this research highlights the potential of NIR laser-induced PCNs as a promising therapeutic tool for treating inner ear dysfunction, particularly vestibular neuropathies, by providing a precise and controlled delivery system for growth factors and safety. While this study confirms the biocompatibility of PCNs in neural progenitor cells and vestibular organoids, potential immune responses and toxicity in complex in vivo environments remain to be fully explored. Although PEG-based nanoparticles are generally associated with low immunogenicity, further studies are needed to assess systemic effects, biodistribution, and long-term safety. These investigations will be essential for validating the clinical feasibility and translational potential of PCNs for sustained therapeutic applications. Further studies and clinical trials are also warranted to validate the efficacy of this approach for clinical applications, with the ultimate goal of improving the quality of life for individuals affected by inner ear disorders. The innovative utilization of nanoparticles, particularly photoresponsive nanoparticles, presents a groundbreaking frontier in addressing inner ear neuropathies. These nanoscale carriers offer unparalleled advantages in targeted drug delivery, providing precise control over therapeutic release while minimizing systemic exposure and maximizing efficacy. The broader range of potential treatment strategies, such as using the PCN as gene or cell delivery tool, is considered the next step.

Supplementary Information

The online version contains supplementary material available at https://doi.org/10.1186/s12951-025-03298-x.

Supplementary Material 1

Author contributions

C.A.: Conceptualization, Methodology, Investigation, Writing- Original Draft, S.R.Y.: Conceptualization, Methodology, Investigation, Writing- Original Draft, Nathaniel Carpena: Methodology, Investigation, Visualization, S.C.A: Methodology, Formal analysis, Software, S.Y.C.: Methodology, Validation, Formal analysis, J.E.C.: Formal analysis, M.Y.L.: Conceptualization, Resources, Data Curation, Visualization, Supervision, Writing- Review & Editing J.Y.J.: Supervision, Project administration.

Funding

This research was supported by the National Research Foundation of Korea (NRF) grant funded by the Ministry of Science and ICT (NRF-2022R1A2C2006358) and supported by Basic Science Research Program through the National Research Foundation of Korea (NRF) funded by the Ministry of Education (NRF-2020R1A6A1A03043283; NRF-2021R1I1A3047407), and supported by Creative Materials Discovery Program through the National Research Foundation of Korea (NRF) funded by Ministry of Science and ICT (NRF-2019M3D1A1078943), and Bio&Medical Technology Development Program of the National Research Foundation (NRF) funded by the Korean government (MSIT) (RS-2023-00220408).

Data availability

No datasets were generated or analysed during the current study.

Declarations

Ethics and consent to participate

Not applicable.

Competing interests

The authors declare no competing interests.

Author details

[1]Beckman Laser Institute Korea, College of Medicine, Dankook University, Cheonan 31116, Republic of Korea
[2]Medical Laser Research Center, College of Medicine, Dankook University, Cheonan 31116, Republic of Korea
[3]Department of Medical Science, Graduate School of Medicine, Dankook University, Cheonan 31116, Republic of Korea
[4]Department of Physiology, College of Medicine, Dankook University, Cheonan 31116, Republic of Korea
[5]Department of Otolaryngology-Head & Neck Surgery, College of Medicine, Dankook University, Cheonan 31116, Republic of Korea

Received: 10 December 2024 / Accepted: 4 March 2025
Published online: 13 March 2025

References

1. Danhier F, Ansorena E, Silva JM, et al. PLGA-based nanoparticles: an overview of biomedical applications. J Control Release. 2012;161(2):505–22.
2. Petros RA, DeSimone JM. Strategies in the design of nanoparticles for therapeutic applications. Nat Rev Drug Discov. 2010;9(8):615–27.
3. Gai S, Yang G, Yang P, et al. Recent advances in functional nanomaterials for light–triggered cancer therapy. Nano Today. 2018;2018(04/01/):19:146–87.
4. Rapp TL, DeForest CA. Targeting drug delivery with light: A highly focused approach. Adv Drug Deliv Rev. 2021 2021/04/01/;171:94–107.
5. Mitchell MJ, Billingsley MM, Haley RM et al. Engineering precision nanoparticles for drug delivery. Nat Rev Drug Discovery. 2021 2021/02/01;20(2):101–24.
6. Cherchi M, Yacovino DA. Histology and neuroanatomy suggest a unified mechanism to explain the distribution of lesion patterns in acute vestibular neuropathy. Exp Brain Res. 2021;239(5):1395–9.
7. Gacek RR, Gacek MR. Vestibular neuronitis: a viral neuropathy. Adv Otorhinolaryngol. 2002;60:54–66.
8. Hegemann SCA, Wenzel A. Diagnosis and treatment of vestibular neuritis/neuronitis or peripheral vestibulopathy (PVP)? Open questions and possible answers. Otol Neurotol. 2017;38(5):626–31.
9. Wang L, Guan J, Wang H, et al. Understanding auditory neuropathy spectrum disorder: a systematic review in Transgenic mouse models. Sci China Life Sci. 2016;59(5):480–6.
10. Rossi G, Manfrin A, Lutolf MP. Progress and potential in organoid research. Nat Rev Genet. 2018;19(11):671–87.
11. Suk JS, Xu Q, Kim N, et al. PEGylation as a strategy for improving nanoparticle-based drug and gene delivery. Adv Drug Deliv Rev. 2016;99(Pt A):28–51.
12. Ernfors P, Van De Water T, Loring J, et al. Complementary roles of BDNF and NT-3 in vestibular and auditory development. Neuron. 1995;14(6):1153–64.
13. Fritzsch B, Tessarollo L, Coppola E, et al. Neurotrophins in the ear: their roles in sensory neuron survival and fiber guidance. Prog Brain Res. 2004;146:265–78.
14. Popper P, Lopez I, Beizai P, et al. Expression of BDNF and TrkB mRNAs in the Crista neurosensory epithelium and vestibular ganglia following ototoxic damage. Brain Res. 1999;846(1):40–51.
15. Xing Y, Zeng B, Yang W. Light responsive hydrogels for controlled drug delivery [Mini Review]. Frontiers in Bioengineering and Biotechnology. 2022 2022-December-16;10.
16. Liu J, Kang W, Wang W. Photocleavage-based photoresponsive drug delivery†. Photochem Photobiol. 2022;98(2):288–302.

17. Liu J, Kang W, Wang W. Photocleavage-based photoresponsive drug delivery. Photochem Photobiol. 2022;98(2):288–302.
18. Di Z, Liu B, Zhao J, et al. An orthogonally regulatable DNA nanodevice for Spatiotemporally controlled biorecognition and tumor treatment. Sci Adv. 2020;6(25):eaba9381.
19. Tewabe A, Abate A, Tamrie M, et al. Targeted drug Delivery - From magic bullet to nanomedicine: principles, challenges, and future perspectives. J Multidiscip Healthc. 2021;14:1711–24.
20. Moon TH, Lee MY, Jung JY, et al. Safety assessment of trans-tympanic photobiomodulation. Lasers Med Sci. 2016;31(2):323–33.
21. Guo W, Patzlaff NE, Jobe EM, et al. Isolation of multipotent neural stem or progenitor cells from both the dentate gyrus and subventricular zone of a single adult mouse. Nat Protoc. 2012;7(11):2005–12.
22. Pacifici M, Peruzzi F. Isolation and culture of rat embryonic neural cells: a quick protocol. J Vis Exp 2012 May 24(63):e3965.
23. Babu H, Claasen JH, Kannan S, et al. A protocol for isolation and enriched monolayer cultivation of neural precursor cells from mouse dentate gyrus. Front Neurosci. 2011;5:89.
24. Liu W, Davis RL. Calretinin and Calbindin distribution patterns specify subpopulations of type I and type II spiral ganglion neurons in postnatal murine cochlea. J Comp Neurol. 2014;522(10):2299–318.
25. Mojumder DK, Wensel TG, Frishman LJ. Subcellular compartmentalization of two calcium binding proteins, calretinin and calbindin-28 kDa, in ganglion and Amacrine cells of the rat retina. Mol Vis. 2008;14:1600–13.
26. Demêmes D, Raymond J, Atger P, et al. Identification of neuron subpopulations in the rat vestibular ganglion by calbindin-D 28K, calretinin and neurofilament proteins immunoreactivity. Brain Res. 1992;582(1):168–72.
27. Xu M, Li S, Xie X et al. ISL1 and POU4F1 directly interact to regulate the differentiation and survival of inner ear sensory neurons. J Neurosci. 2024;44(8).
28. Radde-Gallwitz K, Pan L, Gan L, et al. Expression of Islet1 marks the sensory and neuronal lineages in the mammalian inner ear. J Comp Neurol. 2004;477(4):412–21.
29. Chubinskiy-Nadezhdin VI, Sudarikova AV, Shorokhova MA, et al. Single ion channel recording in 3D culture of stem cells using patch-clamp technique. Biochem Biophys Res Commun. 2022;619:22–6.
30. Alexander JE, Hunt DF, Lee MK, et al. Characterization of posttranslational modifications in neuron-specific class III beta-tubulin by mass spectrometry. Proc Natl Acad Sci U S A. 1991;88(11):4685–9.
31. Limon A, Perez C, Vega R, et al. Ca2+-activated K+-current density is correlated with Soma size in rat vestibular-afferent neurons in culture. J Neurophysiol. 2005;94(6):3751–61.
32. Lang KR, Barnes FS, Daniel JC, et al. Lasers as tools for embryology and cytology. Nature. 1964;201:675–7.
33. Green MA, Zhao J, Wang A, et al. Efficient silicon light-emitting diodes. Nature. 2001;412(6849):805–8.
34. Lee S, Kim HJ, Choi JH, et al. Light emitting diode (LED) irradiation of liposomes enhances drug encapsulation and delivery for improved cancer eradication. J Control Release. 2024;368:756–67.
35. Hong N, Kim HJ, Kang K, et al. Photobiomodulation improves the synapses and cognitive function and ameliorates epileptic seizure by inhibiting downregulation of Nlgn3. Cell Biosci. 2023;13(1):8.
36. Tighilet B, Chabbert C. Adult neurogenesis promotes balance recovery after vestibular loss. Prog Neurobiol. 2019;174:28–35.
37. Travo C, Gaboyard-Niay S, Chabbert C. Plasticity of Scarpa's ganglion neurons as a possible basis for functional restoration within vestibular endorgans. Front Neurol. 2012;3:91.
38. Iyer MR, Ventura C, Bronson D et al. Isolating and culturing vestibular and spiral ganglion Somata from neonatal rodents for Patch-Clamp recordings. J Vis Exp. 2023 Apr 21(194).
39. Hatat B, Boularand R, Bringuier C et al. Effect of Fluoxetine and Acacetin on central vestibular compensation in an animal model of unilateral peripheral vestibulopathy. Biomedicines. 2022;10(9).
40. Zwergal A, Lindner M, Grosch M, et al. In vivo neuroplasticity in vestibular animal models. Mol Cell Neurosci. 2022;120:103721.
41. Baloh RW, Ishyama A, Wackym PA, et al. Vestibular neuritis: clinical-pathologic correlation. Otolaryngol Head Neck Surg. 1996;114(4):586–92.
42. Kerber KA. Chronic unilateral vestibular loss. Handb Clin Neurol. 2016;137:231–4.
43. Patel M, Arshad Q, Roberts RE, et al. Chronic symptoms after vestibular neuritis and the High-Velocity Vestibulo-Ocular reflex. Otol Neurotol. 2016;37(2):179–84.
44. Goddard JC, Fayad JN. Vestibular neuritis. Otolaryngol Clin North Am. 2011;44(2):361-5, viii.
45. Roehm PC, Camarena V, Nayak S, et al. Cultured vestibular ganglion neurons demonstrate latent HSV1 reactivation. Laryngoscope. 2011;121(10):2268–75.
46. Zhao Z, Chen X, Dowbaj AM et al. Organoids Nat Rev Methods Primers. 2022;2.
47. Ji S, Feng L, Fu Z, et al. Pharmaco-proteogenomic characterization of liver cancer organoids for precision oncology. Sci Transl Med. 2023;15(706):eadg3358.
48. Kopalli SR, Behl T, Kyada A et al. Synaptic plasticity and neuroprotection: the molecular impact of flavonoids on neurodegenerative disease progression. Neuroscience. 2025 Feb 6.
49. Yu A, Wang S, Xing Y, et al. 7,8-Dihydroxyflavone alleviates apoptosis and inflammation induced by retinal ischemia-reperfusion injury via activating TrkB/Akt/NF-kB signaling pathway. Int J Med Sci. 2022;19(1):13–24.
50. Mukhopadhyay M, Pangrsic T. Synaptic transmission at the vestibular hair cells of amniotes. Mol Cell Neurosci. 2022;121:103749.
51. Dao HM, Pillai AR, Thakkar R, et al. Near infrared light-induced disassembly of polymeric micelles based on methylene blue conjugated polyethylene glycol. J Appl Polym Sci. 2021;138(2):49665.
52. Dao HM, Whang C-H, Shankar VK, et al. Methylene blue as a far-red light-mediated photocleavable multifunctional ligand [10.1039/C9CC08916K]. Chem Commun. 2020;56(11):1673–6.

Publisher's note